IEEE Access
Multidisciplinary | Rapid Review | Open Access Journal

Received August 7, 2021, accepted August 26, 2021, date of publication August 30, 2021, date of current version September 9, 2021.

Digital Object Identifier 10.1109/ACCESS.2021.3109050

A Comprehensive Review of Control Strategies to Overcome Challenges During LVRT in PV Systems

JYOTI JOSHI[1], ANURAG KUMAR SWAMI[1], VIBHU JATELY[2], (Member, IEEE), AND BRIAN AZZOPARDI[2], (Senior Member, IEEE)

[1]Department of Electrical Engineering, College of Technology, G. B. Pant University of Agriculture and Technology, Pantnagar 263145, India
[2]MCAST Energy Research Group, Institute of Engineering and Transport, Malta College of Arts, Science and Technology, PLA 9032 Paola, Malta

Corresponding author: Jyoti Joshi (jjyotij25@gmail.com)

This work was supported in part by the European Commission H2020 TWINNING Joint Universal activities for Mediterranean PV integration Excellence (JUMP2Excel) Project under Grant 810809.

ABSTRACT Due to the high penetration of grid-connected photovoltaic (GCPV) systems, the network operators are regularly updating the grid codes to ensure that the operation of GCPV systems will assist in maintaining grid stability. Among these, low-voltage-ride-through (LVRT) is an essential attribute of PV inverters that allows them to remain connected with the grid during short-term disturbances in the grid voltage. Hence, PV inverters are equipped with control strategies that secure their smooth operation through this ride-through period as per the specified grid code. However, during the injection of reactive power under LVRT condition, various challenges have been observed, such as inverter overcurrent, unbalance phase voltages at the point of common coupling (PCC), overvoltage in healthy phases, oscillations in active, reactive power and dc-link voltage, distortion in injected currents and poor dynamic response of the system. Several strategies are found in the literature to overcome these challenges associated with LVRT. This paper critically reviews the recent challenges and the associated strategies under LVRT conditions in GCPV inverters. The drawbacks associated with the conventional current control strategies are investigated in MATLAB/Simulink environment. The advanced LVRT control strategies are categorized and analyzed under different types of grid faults. The work categorizes the state-of-the-art LVRT techniques on the basis of the synchronization methods, current injection techniques and dc-link voltage control strategies. It is found that state-of-the-art control strategies like OVSS/OCCIDGS provides improved voltage support and current limitation, which results in smooth LVRT operation by injecting currents of enhanced power quality.

INDEX TERMS Current reference generation, dc-link voltage control, grid-connected PV, low-voltage-ride-through, current limitation, voltage unbalance.

I. INTRODUCTION

During recent years, the penetration of distributed generation (DG) based grid-connected photovoltaic (GCPV) systems have exponentially increased [1]. This is due to its various advantages such as low generation cost, zero carbon emissions, enhancing the grid reliability and alleviating the network capacity. On the other hand, the sporadic power generation of the DG PV system can jeopardize its normal operation leading to voltage variations, increased energy and reactive power losses. Moreover, these PV systems are operated within a specified voltage range, which helps maintain grid stability [2]. Hence, the network operators continuously develop and update the grid codes to minimize the adverse effects of distributed generating resources, like PV, wind, etc., on the power system [3], [4]. Among these grid codes, LVRT is an essential requirement among grid-connected PV inverters. Fundamentally, LVRT is a control action in GCPV inverters that allows them to stay connected with the utility during a short-term sag in the grid voltage [5]–[8]. Under normal operating conditions, the PV system is operated at maximum power point and injects active power into the grid [9]–[12]. However, during LVRT, the large GCPV systems connected at higher voltages inject reactive power to maintain grid stability [13], [14]. Moreover, small capacity GCPV system is generally connected to a low-voltage network and their inverter control action is designed in such a way to give preference to the injection of active power under

The associate editor coordinating the review of this manuscript and approving it for publication was B. Chitti Babu.

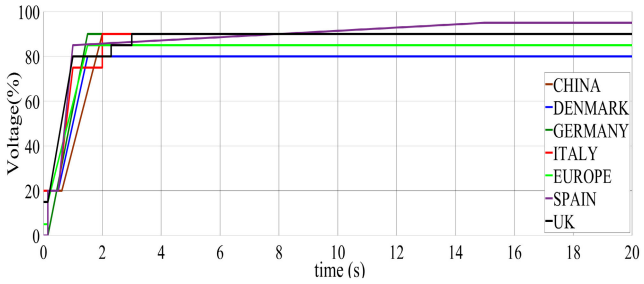

FIGURE 1. LVRT Grid codes in different countries [34].

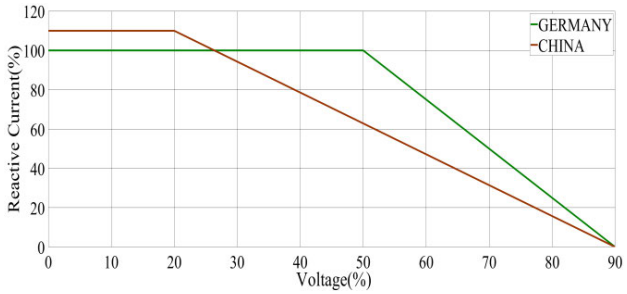

FIGURE 2. Grid codes for reactive power injection [16].

LVRT due to the small X/R ratio of the low-voltage network. To limit the scope of this paper, the authors have reviewed the control strategies that give preference to the injection of reactive power under LVRT.

LVRT requirement is essentially a voltage versus time characteristic, which shows the minimum period required to withstand a voltage drop level. The LVRT of certain grid codes requires an immediate revamping of active and reactive power to the pre-fault values after the voltage has recovered to its nominal value. Other LVRT grid codes require an increased reactive power injection by PVs to provide voltage support to the grid. The operators demand this grid support due to the increasing PV penetration level in the transmission network. Many countries like Germany, China, UK, Italy, Denmark, etc., are continuously updating their LVRT grid codes based on their grid infrastructure to cope with the rapidly expanding use of renewable energy resources, as shown in Figure 1 [15]. According to the German code, the PV inverter should ride through the fault for a maximum of 0.15s under severe faults, i.e., when the grid voltage has dropped to zero. This code allows the PV units to remain connected without any nuisance tripping if the voltage at the point of common coupling (PCC) has been able to recover to 90% of its rated value within 1.5s after a fault. On the other hand, China allows an additional time of 0.475s when the PCC voltage reaches 20% of its rated value. Therefore, the PV units should remain connected for China if the PCC voltage reaches 90% within 2s of its collapse.

Moreover, in German code, if the grid voltage is between 90% – 50%, the DG unit should inject reactive current as a function of voltage sag. If the voltage sag is more than 50%, the DG unit should inject 100% of its reactive current [16]. Chinese grid codes are less stringent as compared to German. The former allows a commensurate reactive power injection when the grid voltage is between 90% – 20%. If the grid voltage falls below 20%, the PV inverters should inject 100% of their reactive power, as shown in Figure 2. This distinction between the German and Chinese grid codes is apparently due to the difference in penetration levels of PV units within these two countries. The Chinese codes may also need revision as the level of distributed generation is on a constant rise in China. The grid codes for various countries under high PV penetration are reviewed in [17], [18].

Several methods are present to enhance the fault ride-through (FRT) capability of PV systems by using additional components like energy storage systems (battery energy storage systems, capacitor energy storage systems), fault current limiters and static synchronous compensator (STATCOM) [19]–[21]. However, the energy storage systems do not consider the injection of reactive current and FACTS devices like STATCOM only inject reactive power to support the grid during fault [22], [23]. Moreover, the overall cost and complexity of the system increase because of the addition of these hardware components. Recently, the researchers have also used computational methods like fuzzy logic control (FLC) and optimization techniques, which help in adjusting the inverter's power references and improve the performance of the inverter controller [24]–[27].

Though these computational methods are efficient and help address the FRT problems, they enhance the system's complexity. However, in light of the issues mentioned above, the modified inverter control techniques are gaining more attention to meet the grid code requirements at a lower cost and better accuracy [28], [29]. Further, the use of these modified inverter control techniques also aids in improving the system speed and its dynamic response [30].

During recent years, several review articles have shone a light on the LVRT capability of GCPV systems [16], [18], [21], [31]–[49]. However, none of the articles have provided a detailed classification and critically reviewed the recently developed modified inverter control techniques for the LVRT capability of PV systems. This paper highlights the differences among the recently published review articles in Table 1 to show the existing research gap clearly.

The proposed work will provide the readers with an exhaustive review of the various control strategies proposed to date that overcome challenges present during LVRT and provide avenues for future work. The key novelty features of the manuscript are:

Certain key objectives are identified that are required during the LVRT condition. Finally, recently developed modified control techniques are classified based on these objectives.

The proposed work has provided a critical review of the various inverter control strategies and their advantages and potential shortcomings.

TABLE 1. Review articles on Low-voltage-ride-through for PV systems.

References	Year	Application	Description
[16]	2018	PV	• Briefly reviewed low-voltage-ride-through, high-voltage-ride-through, low-frequency-ride-through, high-frequency-ride-through and other common grid codes of different countries
[18]	2015	PV	• Suggested improvements required in the existing grid codes for large scale PV adoption in distribution networks
[21]	2019	PV	• Briefly reviewed the conventional fault-ride-through control methods
[31]	2014	PV	• Overview of the challenges associated with LVRT. Brief comparison among PLLs and sequence separation methods
[32]	2015	PV	• Reviewed challenges, stability issues and potential solutions linked with the integration of large-scale PV in transmission and medium voltage distribution system
[33]	2017	Renewable energy sources (RES)	• Compared the conventional inverter current control strategies under unbalanced grid faults by analyzing the behavior of fault current and short-circuit power
[34]	2018	Wind and PV	• Compared fault-ride-through grid codes of 38 countries along with their recent renewable targets
[35]	2018	RES	• Reviewed the LVRT grid-codes, Overview on the potential support devices, control strategies and optimization methods used in reactive power injection to provide grid ancillary services
[36]	2018	PV	• Discussed various methods that provide support functions and ancillary services in smart PV inverters such as reactive power control, fault ride-through and harmonic compensation
[37]	2019	PV	• Overview of grid-codes and control strategies associated with voltage-fault-ride-through adopted in different countries and key aspects present in IEEE1547:2018
[38]	2019	PV	• Conventional reactive power control techniques for three-phase GCPV inverters are compared
[39]	2020	PV	• Reviewed conventional current control techniques, reactive current injection controllers, linear controllers and stability issues associated with these controllers
[40]	2020	PV	• Reviewed the design aspects of low-voltage-ride-through techniques for rooftop PV inverters
[41]	2020	RES	• Discussed the RES integration requirements that provide grid ancillary services and a recommendation on the design of control strategies based on techno-economic assessment
[42]	2020	RES	• Reviewed control strategies for voltage unbalance mitigation in microgrids under islanded and grid-connected mode
[43]	2018	PV	• Compared the current control schemes under different reference frames for single-phase and three-phase PV inverter
[44]	2018	PV	• Compared five voltage support strategies under unbalanced faults during LVRT and HVRT condition
[45]	2020	PV	• Three current limiting approaches are evaluated on a CERTS testbed to highlight their performance
[46]	2016	RES	• Reviewed the state-of-the-art current control techniques for three-phase grid interconnection of renewable power generation systems
[47]	2016	PV	• A comprehensive review on constituents of GCPV systems
[48]	2018	PV	• Compared various dc-link control strategies based on harmonics, reactive power compensation and power factor.
[49]	2020	PV	• Briefly reviewed grid integration standards • Discussed control Strategies for power interface during normal and abnormal grid conditions
[Proposed Work]		PV	• Discussed various issues under LVRT condition in PV systems • Detailed comparison between control strategies to mitigate challenges for smooth operation under LVRT condition based on key performance indices • Future aspects of current and dc-link voltage control strategies to enhance the overall performance of the PV system during LVRT

Since the outer loop dc-link voltage control plays a vital role during LVRT condition, an exhaustive comparison between the recently developed dc-link voltage control strategies along with their potential demerits is presented.

The rest of the paper is organized as: Section II discusses the challenges associated with LVRT. Section III critically reviews the recently developed current control techniques. Section IV classifies and compares various dc-link voltage control strategies along with their merits and demerits. Section V provides a discussion on the future aspects of the control strategies during the LVRT condition. Finally, in Section VI, the conclusion of the work is encapsulated.

II. CHALLENGES UNDER LVRT

As previously discussed, appropriate reactive power is injected into the grid based on the specified grid code to ensure grid stability. The LVRT control action is initiated when the grid voltage drops below its rated value [50]–[54].

Hence, a fast and reliable dip detection method is essential under LVRT condition. This dip detection is usually accomplished by a phase-locked loop (PLL).

Synchronous reference frame-based PLL (SRF-PLL) is commonly used for measuring the RMS values of the grid voltage during normal operating and under balanced fault conditions. A major drawback within the SRF-PLL is its inability to accurately detect the grid voltage dip under unbalanced grid faults.

This inability stems from the presence of negative sequence components, which are rich in higher-order harmonics under unbalanced sag conditions. Several researchers have suggested improvements in conventional SRF-PLL by mainly focusing on increasing the noise elimination capability in the conventional SRF PLL, thereby enhancing their filtering capability [55]–[59].

In [55], a double decoupled synchronous reference frame (DDSRF) based PLL is proposed to detect fundamental frequency positive sequence (FFPS) component of grid voltage under polluted grid conditions. The technique employs a double synchronous reference frame (DSRF) with a decoupling cell which enables the decoupling of positive and negative sequence components. In [56], an improved phase-locked loop (EPLL) is proposed, with enhanced frequency flexibility. The EPLL exhibits superior performance even under frequency divergence of the grid voltage from its theoretical value. This EPLL has a high tolerance to noise and harmonics as compared to the conventional PLL. In [57], a moving average filter (MAF) is used to eliminate the ripples caused by negative sequence components for extracting the fundamental frequency positive sequence (FFPS) component in the synchronous domain. Another attractive approach for synchronization, namely, multiple complex coefficient phase-locked loop (MCCF-PLL), which uses complex coefficient filters (CCFs), is presented in [58]. The CCFs have an inherent property of sequence separation, and therefore, these do not require a sequence separation method or decoupling cell. In [59], a dual second-order generalized integrator (DSOGI) based synchronization technique is presented that evaluates the positive sequence component of grid voltage and eradicates the harmonics during polluted conditions.

Although, PLLs with enhanced filtering capability possess various advantages in accurately detecting the sag in grid voltage, but at a cost of increasing the overall complexity of the system [68]. To overcome this, researchers have formulated control strategies that eliminate the use of PLL [69]. In [70], a control strategy is proposed to overcome the problems related to power quality. As the control technique does not use a phase-locked loop, the system complexity is significantly reduced thereby improving the dynamic response of the system. Another control strategy is suggested for GCPV inverters without using PLL showing satisfactory performance under symmetrical and asymmetrical voltage sag conditions [71]. The proposed control scheme is relatively simpler and free from jitter. A LVRT technique that uses an arbitrary angle instead of a PLL is proposed in [72]. The positive sequence of this angle is obtained by integrating the angular frequency of the grid.

Once a sag in the RMS value of the grid voltage is detected, efficient current reference generation strategies are formulated based on the grid codes [73]. The use of current control strategy helps in limiting the magnitude of the injected currents, mitigating the double grid frequency oscillations within the injected power, providing voltage support at the PCC and ensuring that the injected currents are of low total harmonic distortion (THD) [74]–[76].

Another important task during LVRT under unbalanced fault is to design an efficient dc-link voltage control strategy to prevent inverter shutdown due to overcurrent and to ensure reliable operation of the inverter. This control strategy also prevents overvoltage in the dc-link capacitor during power imbalance occurring under unbalanced fault conditions [77], [78].

To summarize, under LVRT it is essential to quickly detect the voltage dip, initiate appropriate control action to limit the inverter current amplitude as well as determine precise active/reactive power references to provide voltage support at PCC and to ensure power balance. This entails a carefully designed dc-link voltage controller to avoid overvoltage in the dc-link capacitor. Due to the importance of LVRT in PV inverters which contributes toward grid stability, a broad categorization of LVRT techniques is done, based on the following key objectives:

a. Quick dip detection (PLL): Advanced PLLs, notch filters or repetitive controllers are generally used to quickly determine the sag in grid voltage. Several other advanced PLLs have been proposed and reviewed in [60]–[67]. Hence, in this paper, the importance and key attributes of various PLLs which are widely used under LVRT condition, are briefly described in section II.

b. Current control strategy: Formulation of a current control strategy is vital: to limit the amplitude of the injected currents, to provide voltage support and to mitigate double grid-frequency oscillations in injected powers under balanced and unbalanced fault conditions. In this paper, the current control strategies are further classified based on specific objectives that are essential under LVRT.

c. DC-link voltage control: The dc-link voltage control helps in reducing the oscillations in the dc-link capacitor which is detrimental to capacitor life [79]. Moreover, this outer loop control also helps in maintaining the power balance between the dc and ac side. A detailed classification and discussion on the recently developed dc-link voltage control strategies are also carried out ahead.

III. CURRENT REFERENCE GENERATION (CRG)

According to the grid code, a well-designed current reference generation (CRG) must be formulated to deliver the required power components (active and reactive) to the grid [80]. Under normal grid conditions, the objective of the current reference generation strategy is to improve the quality of the power components being injected into the grid

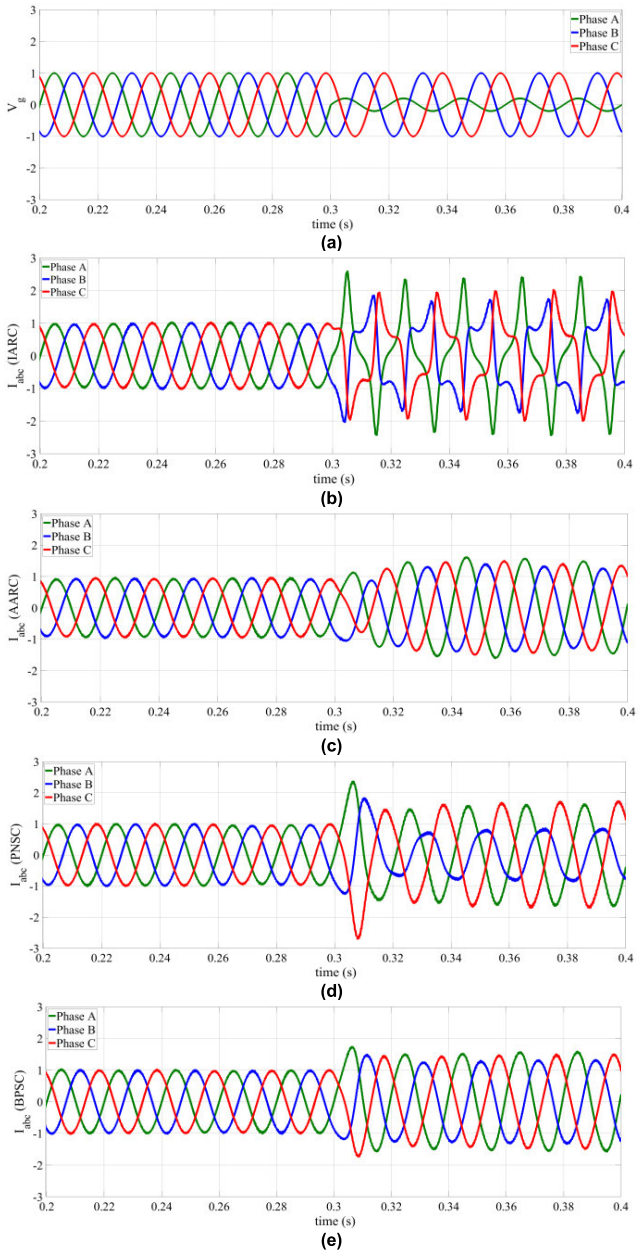

FIGURE 3. Behavior of conventional current reference generation strategies in pu under unbalanced fault for a 2kW GCPV system: (a) Grid voltage, injected currents in (b) IARC, (c) AARC, (d) PNSC and (e) BPSC.

that can be easily delivered by conventional CRG strategies. However, the conventional CRG strategies such as instantaneous active-reactive control (IARC), average active-reactive control (AARC), positive-negative sequence control (PNSC) and balanced positive sequence control (BPSC) require modifications to ensure continuous operation under unbalanced grid faults [81]. This is because these conventional CRG strategies do not provide additional support such as current limitation, voltage support, which are necessary during LVRT operation [82]. It can be observed from Figure 3, that all conventional CRG strategies result in high peak current amplitude under unbalanced grid fault as no provision is made for limiting the peak amplitude of the inverter currents. This can trigger the overcurrent protection devices of the inverter and can result in the disconnection of the PV system. Hence, under unbalanced grid voltage conditions, the major task of the CRG technique during LVRT: is to provide voltage support at the point-of-common coupling (PCC) and to limit the amplitude of the injected currents to ensure continuous safe operation of the PV inverter [83], [84].

The importance of the voltage support, current limitation and dc-link voltage control strategies is explained under two types of faults: unbalanced and balanced grid voltage conditions. In the first case, the strategies are tested under an unbalanced grid voltage condition by reducing the grid voltage of phase A to 0.5pu at t = 0.35s. In the second case, a balanced phase drop in the grid voltage is considered by reducing the phase voltages to 0.5pu at t = 0.35pu.

Since this paper focuses on comparing the recently developed CRG strategies under LVRT conditions, therefore, this article majorly classifies these techniques into two categories based on the objectives stated above in Section II. The current reference generation strategies that are discussed in the following sub-sections can be implemented in stationary, synchronously rotating or natural reference frame as shown in Figure 4.

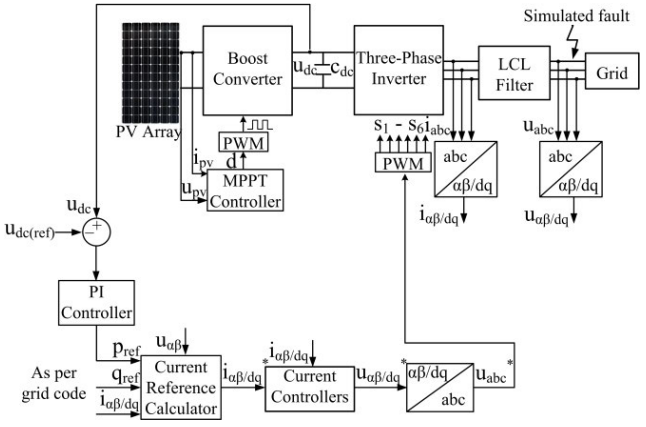

FIGURE 4. Generic circuit diagram of a three-phase two-stage GCPV System.

A. VOLTAGE SUPPORT STRATEGIES (VSS)

According to LVRT grid codes, maximum and minimum voltage limits at the PCC must be specified to ensure the stable operation of GCPV systems under fault conditions. By injecting reactive power, the CRG strategies provide voltage support and help PV systems stay connected to the grid. Under balanced grid voltage sag, the voltage support strategies should be designed to equally raise the voltages in all phases. This is achieved by increasing the positive sequence voltage amplitude at the inverter side. Additionally, the phase voltage equalization is another important objective under unbalanced sag conditions. This is so because an equal rise in the phase voltages can trigger overvoltage

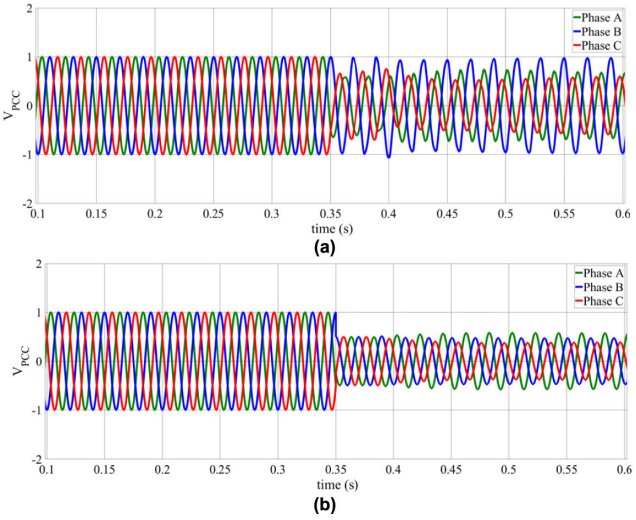

FIGURE 5. Response of voltage support strategy in pu at the PCC under (a) unbalanced and (b) balanced grid faults.

protection, as the healthy phase voltage can easily surpass the maximum permissible voltage limit. By increasing the amplitude of negative sequence voltage, phase equalization is achieved.

The efficient control of the ratio of positive and negative sequence components in the reference currents helps in providing voltage support at the PCC under both unbalanced and balanced types of faults, as shown in Figure 5(a)–(b), respectively.

Hence, a current reference generation strategy that provides voltage support at the PCC should be carefully formulated.

The following sub-sections discuss the recently developed voltage support control strategies during LVRT under balanced and unbalanced grid faults.

1) FLEXIBLE VOLTAGE SUPPORT CONTROL (FVSC) [85]

In [85], [86], a flexible voltage support current reference generation control strategy is proposed. The voltage support is provided by increasing the positive sequence voltage and minimizing the negative sequence of grid voltage, simultaneously, to reduce the unbalance factor (n) in (1).

$$n = \frac{V^-}{V^+} \tag{1}$$

where, $V^+ = \sqrt{v_\alpha^{+2} + v_\beta^{+2}}$,is the positive sequence and $V^- = \sqrt{v_\alpha^{-2} + v_\beta^{-2}}$ is the negative sequence voltage at PCC evaluated under stationary reference frame.

For flexible voltage support, the proposed strategy injects both positive and negative sequence voltage into the grid by adaptively varying their magnitude, under unbalanced grid conditions. The injected reactive current references are formulated as in (2) and (3).

$$i^*_{\alpha q} = \frac{2}{3} Q_{ref} \frac{k^+ v_\beta^+ + k^- v_\beta^-}{k^+ \left(v_\alpha^+\right)^2 + \left(v_\beta^+\right)^2 + k^- \left(v_\alpha^-\right)^2 + \left(v_\beta^-\right)^2} \tag{2}$$

$$i^*_{\beta q} = \frac{2}{3} Q_{ref} \frac{-k^+ v_\beta^+ - k^- v_\beta^-}{k^+ \left(v_\alpha^+\right)^2 + \left(v_\beta^+\right)^2 + k^- \left(v_\alpha^-\right)^2 + \left(v_\beta^-\right)^2} \tag{3}$$

where, k^+ and k^- are the control parameters to balance the positive and negative sequence voltage components, respectively, and $k^- = 1 - k^+$.

Taking the value of k^+ close to 1 will increase the injection of the positive sequence component and result in a constant injection of the negative sequence component. This aids in raising the voltage profile in each phase, under balanced voltage sag. On the other hand, under severe voltage sags, the value of k^+ is chosen close to zero to achieve injection of a constant positive sequence and to decrease the magnitude of the negative sequence component resulting in voltage equalization at the PCC. The positive and negative sequence voltage amplitudes at PCC, are dependent on the voltage drop due to grid side inductance as in (4) and (5), respectively.

$$V^+ = V_g^+ + \frac{2}{3} Q_{ref} \frac{\omega L_g V^+ k^+}{k^+ (V^+)^2 + k^- (V^-)^2} \tag{4}$$

$$V^- = V_g^- - \frac{2}{3} Q_{ref} \frac{\omega L_g V^- k^-}{k^+ (V^+)^2 + k^- (V^-)^2} \tag{5}$$

where, ω is the grid angular frequency and Q_{ref} is the reactive power reference. L_g is the grid side inductance, whereas, V_g^+ and V_g^- are the positive and negative sequence component of the grid voltage, respectively.

Although the proposed strategy provides enhanced voltage support, evidently it demands the calculation of grid impedance. Moreover, within this strategy, the maximum allowable inverter current that can be injected into the grid has not been considered.

2) VOLTAGE SUPPORT CAPABILITY IN DISTRIBUTED GENERATED INVERTERS (VSCDGI) [87]

A strategy is proposed in [85] to equally raise the phase voltage without designing a voltage control loop. This is a major drawback as the reference reactive power Q_{ref} and the control parameter k^+ are calculated without the knowledge of PCC voltage. As previously discussed, for stable operation the maximum and minimum values of phase voltages should be within the limits as per the specified grid codes. To this effect, a method is proposed in [87] which employs a voltage control loop to determine the values of Q_{ref} and k^+ in (6) and (7), respectively.

$$Q_{ref} = \frac{3}{2} \frac{V_p^*(V_p^* - V_{gp}) - V_n^*(V_n^* - V_{gn})}{\omega L_g} \tag{6}$$

$$k^+ = \frac{V_n^*(V_p^* - V_{gp})}{V_p^* V_{gn} - V_n^* V_{gp}} \tag{7}$$

where, V_p^* and V_n^* are the references for positive and negative sequence voltages at PCC, respectively. V_p^* and V_n^* are determined from the type of sag characteristic based on the lower (V_L^*) and upper (V_H^*) boundary values, where, $V_L^* = \min(V_a, V_b, V_c)$ and $V_H^* = \max(V_a, V_b, V_c) = (V_L^* + \Delta V)$. where, $\Delta V = \max(V_a, V_b, V_c) - \min(V_a, V_b, V_c)$. V_{gp} and V_{gn} is the positive and negative sequence component of the grid voltage, respectively.

To provide better voltage support, the reactive reference currents are formulated, in $\alpha\beta$ reference frame as in (8)-(9).

$$i_{\alpha q}^* = \frac{2}{3}\frac{k^+ v_\beta^+ + (1-k^+)v_\beta^-}{k^+\left(V^+\right)^2 + (1-k^+)\left(V^-\right)^2} Q_{ref} \tag{8}$$

$$i_{\beta q}^* = -\frac{2}{3}\frac{k_q v_\alpha^+ + (1-k_q)v_\alpha^-}{k^+\left(V^+\right)^2 + (1-k^+)\left(V^-\right)^2} Q_{ref} \tag{9}$$

where, k^+ is the balancing factor which can take any value between 0 and 1.

3) REACTIVE POWER CONTROL OF DISTRIBUTED GENERATION INVERTERS (RPCDGI) [88]

In [87], the strategy was primarily focused on providing voltage support under symmetrical voltage sags. In [88], this limitation was overcome by proposing a control strategy that works well under unbalanced grid voltage conditions too. The technique increases the positive sequence voltage component by injecting the positive sequence reactive power through the inductor which in turn increases the PCC voltage by a voltage variation of $\omega L_g I^+$. On the contrary, to reduce the negative sequence component of the PCC voltage, the negative sequence reactive power is injected which reduces the PCC voltage by $\omega L_g I^-$. By simultaneously, raising and reducing the positive and negative sequence voltage, respectively, the voltage unbalance is minimized. The CRG equations to flexibly regulate the positive and negative reactive power are given in (10) and (11).

$$i_\alpha^* = \frac{2}{3}\left[\frac{v_\beta^+}{\left(v_\alpha^+\right)^2 + \left(v_\beta^+\right)^2} Q^+ + \frac{v_\beta^-}{\left(v_\alpha^-\right)^2 + \left(v_\beta^-\right)^2} Q^-\right] \tag{10}$$

$$i_\beta^* = -\frac{2}{3}\left[\frac{v_\alpha^+}{\left(v_\alpha^+\right)^2 + \left(v_\beta^+\right)^2} Q^+ + \frac{v_\alpha^-}{\left(v_\alpha^-\right)^2 + \left(v_\beta^-\right)^2} Q^-\right] \tag{11}$$

Further to ensure the PCC voltages stay within the limit, the positive and negative sequence reactive power references are formulated in (12) and (13), respectively.

$$Q^+ = \frac{3}{2}\frac{\left(V^+\right)^*\left[\left(V^+\right)^* - V_g^+\right]}{\omega L_g} \tag{12}$$

$$Q^- = \frac{3}{2}\frac{\left(V^-\right)^*\left[\left(V^-\right)^* - V_g^-\right]}{\omega L_g} \tag{13}$$

where, $\left(V^+\right)^*$ and $\left(V^-\right)^*$ are the desired positive and negative sequence voltages, respectively and are further evaluated by carefully determining the maximum and minimum value between phase voltages.

4) FLEXIBLE VOLTAGE SUPPORT WITH IMBALANCE MITIGATION IN DISTRIBUTED GENERATION INVERTERS (FVSDGI) [89]

In [89], the injection of reactive current by using a three-level T-type inverter for medium switching frequency and low-voltage applications, has been considered. The proposed strategy employed DDSRF-PLL to extract the positive and negative sequence current components at PCC. The reference currents are generated by combining both positive and negative sequence components of PCC currents and are in accordance with the maximum and minimum voltage limits at PCC. Under balanced voltage sags, the PCC voltages are equally raised with the help of a positive sequence regulator. On the other hand, under unbalanced voltage conditions, two PCC voltage setpoints are determined and flexible control of both positive and negative sequence current regulator helps in achieving voltage equalization. Under deep voltage sag conditions, a current saturation strategy is activated which helps in only injecting the positive sequence current thereby avoiding overcurrent. The active and reactive current references in d-q reference frame are formulated as in (14) and (15), respectively.

$$\left(i_d^+\right)^* = 0 \tag{14}$$

$$\left(i_q^+\right)^* = -(I^+)^* \tag{15}$$

As shown in (14)-(15), under severe grid fault conditions the injection of active current is taken as zero, hence only reactive current injection is considered.

$$\left(i_d^-\right)^* = \left(I^-\right)^*\left(\frac{\bar{v}_q^-}{V^-}\right) \tag{16}$$

$$\left(i_q^-\right)^* = \left(I^-\right)^*\left(-\frac{\bar{v}_d^-}{V^-}\right) \tag{17}$$

In (16)-(17) , $\bar{v}_d^-$ and $\bar{v}_q^-$ are the filtered negative sequence voltages in d-q reference frame. $\left(I^+\right)^*$ and $(I^-)^*$ are reference of positive and negative current amplitude, respectively, obtained from voltage control loop, whereas V^- is the phasor sum of negative sequence filtered voltages in d-q reference frame.

5) INDIVIDUAL PHASE CURRENT CONTROL TO AVOID OVERVOLTAGE (IPCC) [90]

It is evident that random injection of positive and negative sequence components without monitoring the voltage drop in each phase can result in overvoltage in healthy phases. In [90], a scheme is proposed to avoid overvoltage in healthy phases by independently controlling the current in each phase. Evidently, the injection of balanced reactive currents under unbalanced voltage sags results in overvoltage in healthy phases, hence, the strategy is based on updated European grid code which requires the injection of unbalanced reactive currents to assist towards grid stability [91]. The injection of reactive current is based on the amount of voltage drop in the faulty phase to ensure that the healthy

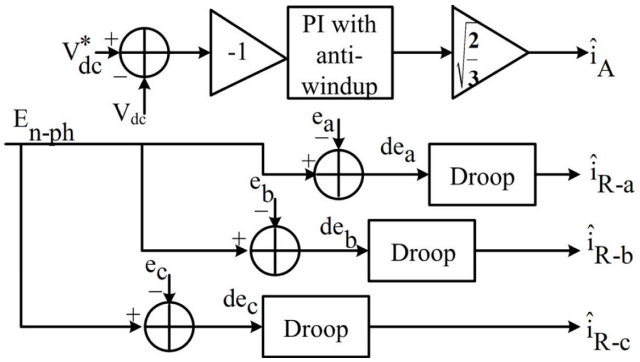

FIGURE 6. Block diagram for active and reactive current references.

phases remain unaffected. The reactive current is obtained as the output of the droop controller and is given as in (18).

$$\hat{i}_{R-x} = droop\,|de_x|\,\hat{I}_n, \quad \text{where x} \in (a, b, c) \tag{18}$$

where, droop coefficient is a constant and is evaluated as per the grid codes, de_x is the amount of deviation in the phase voltage from the nominal value and $\hat{I}_n$ is the nominal current of the inverter as shown in Figure 6.

6) ADVANCE VOLTAGE SUPPORT CONTROL (AVSC) [92]

In [92], a strategy is proposed which is suitable for both inductive and resistive grids and hence injects both active and reactive power into the grid during fault conditions.

Under unbalanced grid voltage conditions, the VSS limits the phase voltages at PCC by setting the maximum and minimum voltage limits according to the grid codes. The positive and negative sequence reference currents for active and reactive power for any X/R ratio are given in (19) – (22), respectively.

$$I_p^+ = \frac{R_g}{X_g^2 + R_g^2} \times \Delta V_{ref}^+ \tag{19}$$

$$I_p^- = \frac{R_g}{X_g^2 + R_g^2} \times \Delta V_{ref}^- \tag{20}$$

$$I_q^+ = \frac{X_g}{X_g^2 + R_g^2} \times \Delta V_{ref}^+ \tag{21}$$

$$I_q^+ = \frac{-X_g}{X_g^2 + R_g^2} \times \Delta V_{ref}^- \tag{22}$$

where, ΔV_{ref}^+ and ΔV_{ref}^- are the positive and negative sequence voltage drop, respectively, due to the grid-side inductance and resistance. X_g and R_g are the inductance and resistance of grid, respectively. It is evident from (19)-(22), for the inductive grid, there is no contribution from the active current component. For such an instance, this strategy aims to inject maximum active power and regulates the phase voltages, simultaneously. However, the injected active power would suffer from oscillations under severe unbalanced grid conditions.

7) POSITIVE AND NEGATIVE SEQUENCE VOLTAGE SUPPORT STRATEGY (PNSVSS) [93]

In [93], a strategy is designed for both inductive and resistive grids which helps in raising the positive sequence voltage, reducing the negative sequence voltages, and maximizing the difference between these two sequences. The increase in the positive sequence component helps in raising the voltage magnitude and reducing the negative sequence component aids towards phase equalization. The additional objective of maximizing the difference between these two sequences ensures full utilization of inverter capacity as it injects the rated current as well as provides voltage support.

The active and reactive reference currents are formulated as in (23)-(26).

$$i^*_{\alpha(p)} = \frac{2}{3}\left[\frac{v_\alpha^+}{\left(v_\alpha^+\right)^2 + \left(v_\beta^+\right)^2}P^+ + \frac{v_\alpha^-}{\left(v_\alpha^-\right)^2 + \left(v_\beta^-\right)^2}P^-\right] \tag{23}$$

$$i^*_{\beta(p)} = \frac{2}{3}\left[\frac{v_\beta^+}{\left(v_\alpha^+\right)^2 + \left(v_\beta^+\right)^2}P^+ + \frac{v_\beta^-}{\left(v_\alpha^-\right)^2 + \left(v_\beta^-\right)^2}P^-\right] \tag{24}$$

$$i^*_{\alpha(q)} = \frac{2}{3}\left[\frac{v_\beta^+}{\left(v_\alpha^+\right)^2 + \left(v_\beta^+\right)^2}Q^+ + \frac{v_\beta^-}{\left(v_\alpha^-\right)^2 + \left(v_\beta^-\right)^2}Q^-\right] \tag{25}$$

$$i^*_{\beta(q)} = \frac{2}{3}\left[\frac{-v_\alpha^+}{\left(v_\alpha^+\right)^2 + \left(v_\beta^+\right)^2}Q^+ + \frac{-v_\alpha^-}{\left(v_\alpha^-\right)^2 + \left(v_\beta^-\right)^2}Q^-\right] \tag{26}$$

The amplitude of positive and negative sequence voltage at the PCC is obtained as in (27) and (28), respectively.

$$V^+ = R_g I_p^+ + \omega L I_q^+ + \sqrt{\left(V_g^+\right)^2 - \left(\omega L I_p^+ - R_g I_q^+\right)^2} \tag{27}$$

$$\mathrm{V}^- = R_g I_p^- - \omega L I_q^- + \sqrt{\left(V_g^-\right)^2 - \left(\omega L I_p^- - R_g I_q^-\right)^2} \tag{28}$$

where, I_p^+, I_q^+, I_p^- and I_q^- are the positive and negative sequence components of active and reactive currents, respectively.

8) MAXIMIZING VOLTAGE SUPPORT IN LOWEST PHASE (MVSLP) [94]

In [94], [95], a voltage support strategy is proposed by maximizing the RMS value of the most sagged phase voltage and reducing the risk of an under-voltage disconnection, during unbalanced grid sag conditions. The scheme works well regardless of the grid impedance and maximizes the inverter's capability by injecting the rated current. The reference currents are formulated as in (29)-(30).

$$i_\alpha^* = \frac{I_p^+}{V^+}v_\alpha^+ + \frac{I_q^+}{V^+}v_\beta^+ \tag{29}$$

$$i_\beta^* = \frac{I_p^+}{V^+}v_\beta^+ - \frac{I_q^+}{V^+}v_\alpha^+ \tag{30}$$

It can be observed from (29)-(30), that balanced currents are injected into the grid, as only the positive sequence component is being considered. Hence, voltage imbalance remains the major drawback of this method.

9) MAXIMIZE REACTIVE CURRENT INJECTION TO AVOID OVER VOLTAGE (MRCAO) [97]

In [96], the strategy ensures simultaneous injection of the maximum value of the positive sequence component of the reactive current to achieve maximum voltage rise in the faulted phase and the injection of negative sequence component of the reactive current to ensure phase equalization. The major demerit of this strategy is that it requires a reliable evaluation of the grid impedance and the controller operates in the open-loop. To overcome this drawback, a voltage control loop is incorporated in [97] to avoid overvoltage in healthy phases. The strategy uses two PI controllers, one to inject the maximum rated current in the disturbed phase, and the other to avoid overvoltage in healthy phases. The current reference generation equations are formulated by using the normalized values of the positive and negative sequence voltages as in (31) and (32).

$$i_\alpha^* = \frac{I_p}{V^+} v_\alpha^+ + \frac{I_q^+}{V^+} v_\beta^+ + \frac{I_q^-}{V^-} v_\beta^- \tag{31}$$

$$i_\beta^* = \frac{I_p}{V^+} v_\beta^+ - \frac{I_q^+}{V^+} v_\alpha^+ - \frac{I_q^-}{V^-} v_\alpha^- \tag{32}$$

Here I_p, helps in injecting the active power, I_q^+ is used to balance the phase currents and I_q^- prevents overvoltage in the healthy phase.

10) MULTIPLE OBJECTIVE VOLTAGE SUPPORT STRATEGY (MOVSS) [98]

In [98], a similar VSS is proposed for inductive and resistive grids that minimize the imbalance in voltage by reducing and increasing the negative and positive sequence component of reactive power, respectively as in (33) and (34).

$$\Delta V^+ = V_g^+ - V_{PCC}^+ = R_g I_d^+ + \omega L_g I_q^+ \tag{33}$$

$$\Delta V^- = V_g^- + V_{PCC}^+ = R_g I_d^- - \omega L_g I_q^- \tag{34}$$

$\Delta V+$ and $\Delta V-$ determine the voltage support from the utility to the point of common coupling. The positive and negative sequence of active and reactive reference currents are formulated in SRF as in (35)-(38).

$$i_d^+ = \frac{2}{3}\frac{P^+}{V_{PCC}^+} \tag{35}$$

$$i_d^- = \frac{2}{3}\frac{P^-}{V_{PCC}^-} \tag{36}$$

$$i_q^+ = \frac{2}{3}\frac{Q^+}{V_{PCC}^+} \tag{37}$$

$$i_d^- = \frac{2}{3}\frac{Q^-}{V_{PCC}^-} \tag{38}$$

The increment in the positive sequence and decrement in the negative sequence component of PCC voltage is achieved by carefully determining the reactive power references as in (39) and (40), respectively.

$$Q^+ = \frac{3}{2}\frac{R_g}{X_g^2 + R_g^2} \times V_{PCC}^+ \Delta V^+ \tag{39}$$

$$Q^- = -\frac{3}{2}\frac{R_g}{X_g^2 + R_g^2} \times V_{PCC}^- \Delta V^- \tag{40}$$

11) OPTIMAL VOLTAGE SUPPORT STRATEGY (OVSS) [99]

Similar to strategies proposed in [93]–[98], the control strategy in [99] is also based on the minimization of voltage unbalance factor (n). However, the optimal solution is obtained based on the knowledge of the impedance angle of the injected current as in (41).

$$\theta_{inj} = \theta_g = tan^{-1}\frac{\omega L_g}{R_g} \tag{41}$$

The optimal positive sequence active and reactive current references are given by (42) and (43), respectively.

$$i_p^+ = i_{p(opt)}^+ = I\cos\theta_{inj} \tag{42}$$

$$i_q^+ = i_{q(opt)}^+ = I\cos\theta_{inj} \tag{43}$$

where, I is a predetermined current value that will limit the amplitude of the inverter current. Based on (42) and (43), the positive and negative sequence components of PCC voltage are determined as in (44) and (45), respectively.

$$V^+ = V_g^+ + I\sqrt{R_g^2 + \left(\omega L_g\right)^2} \tag{44}$$

$$\mathrm{V}^- = V_g^- - nI\sqrt{R_g^2 + \left(\omega L_g\right)^2} \tag{45}$$

Apart from the above-mentioned VSS, several other improvements have been proposed to provide enhanced voltage support under unbalanced faults [100]–[105]. In [100], the injection of both active and reactive current is based on the severity of voltage sags so that the inverter rating is not exceeded. In [101], the voltage unbalance factor is minimized by employing droop control. The scheme injects the positive and negative sequence components of active and reactive powers to ensure that the PCC voltage remains within specified limits. A symmetric component decoupled control strategy (SCDCS) for a three-phase four-wire system is proposed in [102]. The strategy injects the active power by utilizing the positive sequence component of the inverter current. Moreover, the negative and zero sequence components are utilized to provide local voltage support and unbalance correction. It can be concluded that the knowledge of grid impedance is imperative in deciding the proper VSS i.e., for an inductive grid, the injection of reactive power is preferred which helps in raising the phase voltages as opposed to the preference given to the injection of active power for a resistive grid [103]. In [104], a model predictive current controller (MPCC) is proposed to enhance the VSS under different grid faults. In this controller, the voltage limit targets

TABLE 2. Comparison between voltage support strategies under low-voltage-ride-through condition.

Reference, Strategy	Type of grid	Controller	Experiment results	Advantages	Disadvantages	THD	Efficiency	Accuracy	Power Factor	Network Losses	Dynamic Response
[85], FVSC	Inductive	Proportional Resonant (PR)	Yes	• Flexible voltage support	• Knowledge of grid impedance is required • The maximum allowable current to the grid is not considered • Voltage limitation is not specified	Low	High	Low	High	High	Excellent
[87], VSCDGI	Inductive	PR	Yes	• Voltage control loop is designed that specifies the minimum and maximum voltage limits • Reactive power support for low current injection than maximum acceptable rating	• Only symmetrical faults are considered • Delay in execution time to control voltage sags	Low	High	High	Unity	Low	Poor
[88], RPCDGI	Inductive	PR	Yes	• Can be used under both symmetrical and asymmetrical faults • Improved dynamic response • Time varying grid faults are incorporated within this strategy	• Only reactive power is injected to the grid	High	Low	Low	Low	Low	Poor
[89], FVSDGI	Inductive	Proportional Integral (PI)	Yes	• Estimation of grid impedance is not required which reduces the complexity	• Requires the use of an advance PLL • Challenge in tuning the controller parameters	Low	High	Low	High	Low	Excellent
[90], IPCC	Inductive	PR	Yes	• Individual phase currents are controlled hence overvoltage in healthy phases is absent	• The system performance with PR controllers, is poor under variation of the system frequency as it provides infinite gain at the selected harmonic frequencies	Low	High	High	High	High	Excellent
[92], AVSC	Resistive & inductive	PR	Yes	• Active power injection is taken into account • Compensation of zero sequence voltage results in improved accuracy	• Large active power oscillations under unbalanced grid conditions	Low	Low	High	High	High	Excellent
[93], PNSVSS	Resistive & inductive	PR	Yes	• Maximizing the difference between positive and negative sequence voltage helps in exploiting the full capacity of inverter	• Estimation of grid impedance is essential	Low	Low	High	High	High	Poor
[94], MVSLP	Resistive & Inductive	PR	Yes	• Additional voltage support is provided to the most faulty phase and avoids the under voltage disconnection • Rated current of the inverter is injected	• Grid impedance estimation is vital	Low	Low	High	High	Low	Poor
[96], RCIPVS	Inductive	PR	Yes	• Strategy can be applied in low power rating distributed generation systems • Voltage equalization is achieved • Maximum reactive current is injected to support the phase with lowest amplitude	• Application is limited to inductive grids • Over current can lead to disconnection • Active and reactive power contains sustained oscillations	High	High	High	Low	Low	Poor
[97], MRCAO	Inductive	PI and PR	Yes	• Voltage control loop is designed to avoid overvoltage in healthy phase • Over current control and voltage control is achieved simultaneously • Low computational burden	• Reactive power contains sustained oscillations	High	High	High	Low	Low	Excellent
[98], MOVSS	Resistive & Inductive	Proportional complex integral (PCI)	No	• Simultaneous injection of both active and reactive power • Small oscillations in active power and dc-link voltage. • Minimizes overcurrent in inverter	• Tuning of proportional integral controller is challenging	Low	High	High	High	Low	Excellent
[99], OVSS	Resistive & Inductive	PR	Yes	• Avoids active power oscillations • Injected current amplitude is controlled • Maximizes the difference between positive sequence voltage and negative sequence voltage to utilize the capacity of inverter	• Calculation of grid impedance is imperative	Low	High	High	High	Low	Excellent
[100], VSSSE	Resistive & Inductive	PI	No	• Inverter capacity is utilized and current limitation is provided	• Voltage unbalance correction is not considered	High	Low	Low	Low	Low	Excellent
[101], VSSDC	Inductive	Quasi PR	Yes	• Lower and Upper voltage limits are specified	• Distorted currents are injected to the grid	High	High	High	Low	Low	Excellent
[102], SCDS	Inductive	PI	Yes	• Use of negative and zero sequence component improves unbalance between phases	• Harmonics in the injected currents are higher as compared to other advanced strategies	Low	Low	Low	High	High	Excellent
[104], AVSSZSV	Resistive & Inductive	MPPC	Yes	• High flexibility in control due to additional control variables • A four-leg NPC inverter topology is employed to support the PCC voltage	• Injected currents are unbalanced	Low	High	Low	High	Low	Excellent

are achieved by including the zero-sequence component of voltage in the current references. An improved communication-less control strategy for voltage unbalance mitigation is proposed in [105]. In this scheme, the grid impedance estimation is not required and the LV network is imitated by choosing the line impedances to ensure that the X/R ratio is selected close to one. The above-mentioned voltage support strategies are compiled based on certain key performance parameters in Table 2.

B. CURRENT LIMITATION STRATEGIES (CLS)

Another challenge that exists under low-voltage-ride-through condition is to ensure that the peak amplitude of the inverter currents does not exceed beyond the inverter rated capacity. To elaborate on this concept, consider if there is a short-term voltage sag in one of the grid phases. To ensure power balance between dc and ac network the faulty phase inverter current increases and keeps injecting the same power coming from the dc side. If the amplitude of the faulty phase current exceeds beyond the rating of the inverter, protection devices within the inverter will switch off the inverter for its safety. This interruption in the operation of the inverter will prevent the ride-through operation of the PV inverter. Hence, the current limitation is an important objective under LVRT that limits the amplitude of the injected currents to the rated value, to avoid the operation of overcurrent protection devices. The response of current limitation strategies under unbalanced and balanced grid faults are shown in Figure 7 (a) and (b), respectively. In the following sub-sections various control strategies are discussed that provide over current limitation under balanced and unbalanced grid faults.

1) TWO DISCRETE PARAMETER CONTROL (TDPC) [106]

In [106], a current control strategy is proposed which formulates a generalized current reference expression by combining various conventional CRG techniques with the help of two discrete control parameters (α, β). The optimum power quality characteristics can be obtained by carefully choosing the values of α and β in the range of (-1, 1). To obtain the optimum power quality characteristics for a specific condition, values of α and β can be used for the chosen CRG strategy as given in Table 3.

In [99], reference equations are formulated as in (46)-(48).

$$i_{ref} = i^{+}_{ref} + i^{-}_{ref} \tag{46}$$

$$i^{+}_{ref} = \frac{Pv^{+}}{\left|v^{+}\right|^{2} + (1+\alpha)\,\beta v^{+}v^{-} + \alpha\left|v^{-}\right|^{2}} \tag{47}$$

$$i^{-}_{ref} = \frac{\alpha P v^{-}}{\left|v^{+}\right|^{2} + (1+\alpha)\,\beta v^{+}v^{-} + \alpha\left|v^{-}\right|^{2}} \tag{48}$$

where, i^{+}_{ref} and i^{-}_{ref} are the positive and negative sequence reference current vectors, respectively and P indicates the active power reference. By replacing the different values of α and β in (46)-(48), conventional current schemes can be obtained. This type of flexible control strategy can be most promising to meet future LVRT requirements. Although efficient, this strategy does not provide any regulation on the minimum set point in the reduction of the inverter overcurrent.

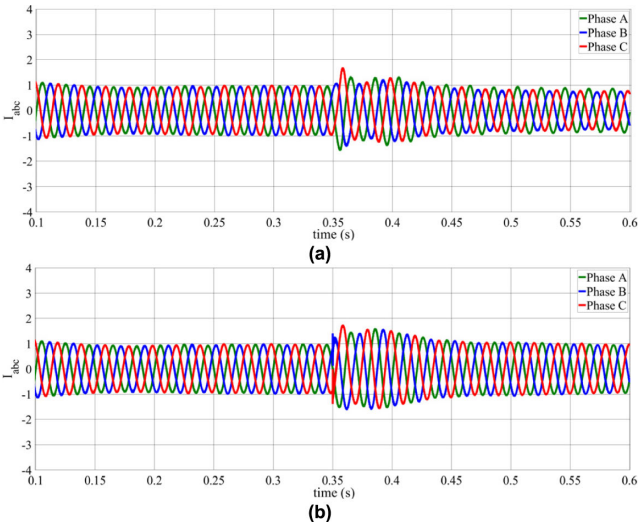

FIGURE 7. Response of current limitation strategy in pu at the PCC under (a) unbalanced and (b) balanced grid faults.

TABLE 3. Values of α, β for conventional CRG strategies.

Strategy	α	β
IUPFC	1	1
PNSC	−1	1
AARC	1	0
BPSC	0	0

2) MINIMUM PEAK GRID INJECTION CURRENT CONTROL (MPGICC) [107]

In [107], a strategy is proposed to minimize the power quality problems and help in determining the minimum peak currents during polluted grid conditions. The instantaneous phase currents are obtained as in (49)-(51).

$$i_a = \frac{2}{3}\cdot\frac{P^*}{V^+}\cdot\frac{(1+\alpha n\cos\omega t)}{1+\beta\,(1+\alpha)\,n\cos\,(2\omega t)+\alpha n^2} \tag{49}$$

$$i_b = \frac{2}{3}\cdot\frac{P^*}{V^+}\cdot\frac{\cos\left(\omega t-\left(\frac{2\pi}{3}\right)\right)+\alpha n\cos\left(\omega t+\left(\frac{2\pi}{3}\right)\right)}{1+\beta\,(1+\alpha)\,n\cos\,(2\omega t)+\alpha n^2} \tag{50}$$

$$i_c = \frac{2}{3}\cdot\frac{P^*}{V^+}\cdot\frac{\cos\left(\omega t+\left(\frac{2\pi}{3}\right)\right)+\alpha n\cos\left(\omega t-\left(\frac{2\pi}{3}\right)\right)}{1+\beta\,(1+\alpha)\,n\cos\,(2\omega t)+\alpha n^2} \tag{51}$$

where, P^*, is the reference power signal and n is the voltage unbalance factor (VUF) of (1), which can take any value between 0-1. It is evident from (49)-(51) that the peak values of the currents are dependent on the values of α and β. By precisely choosing the values of these two control parameters, the peak currents are minimized. The proposed scheme is extremely useful in balanced conditions, however, during longer periods of voltage sags of more than one second,

the injected currents are distorted due to the presence of negative sequence component.

3) REDUCE RISK OF OVERCURRENT PROTECTION (RROCP) [108]

Based on the conventional positive-negative sequence control (PNSC) method, the strategy in [108] injects negative sequence inductive currents to effectively control the peaks in the current waveforms. The peak currents of the three phases are formulated as in (52) – (54).

$$I_{aPeak} = \sqrt{\left(I_p^2 + I_n^2 + 2I_pI_n\cos\varphi\right)} \tag{52}$$

$$I_{bPeak} = \sqrt{\left(I_p^2 + I_n^2 + 2I_pI_n\cos\left(\varphi + \frac{4\pi}{3}\right)\right)} \tag{53}$$

$$I_{bPeak} = \sqrt{\left(I_p^2 + I_n^2 + 2I_pI_n\cos\left(\varphi - \frac{4\pi}{3}\right)\right)} \tag{54}$$

where,

$$\varphi = \emptyset_2 - \emptyset_n - \emptyset_1 - \emptyset_p$$
$$\emptyset_1 = -\tan^{-1}\frac{v_d^+}{v_q^+}, \quad \emptyset_2 = -\tan^{-1}\frac{v_d^-}{v_q^-} \quad \text{and}$$
$$\emptyset_n = -\frac{\pi}{2}, \quad \emptyset_p = -\tan^{-1}\frac{i_d^+}{i_q^+} \tag{55}$$

where, v_d^+, v_q^+, v_d^- and v_q^- are the positive and negative sequence component of grid voltages, respectively, in the synchronously rotating reference frame. Similarly, i_d^+, i_q^+, i_d^- and i_q^- are the positive and negative sequence component of grid currents, respectively. $\emptyset_1$ and $\emptyset_2$ are the phase angles of the positive and negative sequence voltages with respect to the reference axis. $\emptyset_p$ and $\emptyset_n$ are the phase angles of the positive and the negative sequence currents, respectively, whereas I_p and I_n are obtained using (56) and (57), respectively.

$$I_p = \left(i_d^+\right)^2 + \left(i_q^+\right)^2 \tag{56}$$

$$I_n = i_d^- \tag{57}$$

It can be observed from (52)-(54), that the peak values of the currents are dependent on φ. To limit the peak amplitude, the phase currents should not exceed the maximum value of current I_{max} from (58) and hence I_{max} is set below the threshold value to avoid the operation of overcurrent protection.

$$I_{max} = \max\left(I_{aPeak}, I_{bPeak}, I_{cPeak}\right) \tag{58}$$

4) ZERO SEQUENCE CURRENT CONTROL (ZSCC) [109]

In [109], a control strategy is proposed by considering zero-sequence component to ameliorate the power quality issues in a grid-connected distributed generation system. Normally, the conventional current control schemes have four control variables (i_d^+, i_q^+, i_d^- and i_q^-) in a three-wire system. The control strategy of [109] has six control variables ($i_d^+, i_q^+, i_d^-, i_q^-, i_{Re}^0$ and i_{Im}^0) for a four or six-wire converter system to achieve better performance under unbalanced grid conditions. With the injection of the zero-sequence current component, two additional controls of freedom are obtained to improve the power quality characteristics.

The scheme is essentially divided into two objectives: objective 1, in which the oscillations in active and reactive power are removed and objective 2, where the oscillations in active power and negative sequence current are eliminated at the same time. The current references for objective 1 are given as in (59)-(62).

$$i_d^+ = \frac{2}{3}\cdot\frac{P^*}{\left(v_d^+ - v_d^-\right).\left(1 - v_d^-/v_d^+\right)}; \quad i_d^- = \frac{v_d^-}{v_d^+}.i_d^+ \tag{59}$$

$$i_q^+ = \frac{2}{3}\cdot\frac{Q^*}{-v_d^+ + \left(v_d^-\right)^2/v_d^+}; \quad i_q^- = -\frac{v_d^-}{v_d^+}.i_q^+ \tag{60}$$

$$i_{Re}^0 = \frac{2}{3}\cdot\frac{P^* - \bar{P}}{v_{Re}^0} \tag{61}$$

$$i_{Im}^0 = \frac{v_d^+.i_q^- - v_d^-.i_q^+}{v_{Re}^0} \tag{62}$$

Using (59)-(62), the oscillations in active and reactive power can be eliminated. On the other hand, the reference currents for objective 2 are given as in (63)-(66).

$$i_d^+ = \frac{2}{3}\cdot\frac{P^*}{\left(v_d^+ - v_d^-\right)}; \quad i_d^- = 0 \tag{63}$$

$$i_q^+ = \frac{2}{3}\cdot\frac{Q^*}{-v_d^+}; \quad i_q^- = 0 \tag{64}$$

$$i_{Re}^0 = \frac{-v_d^-.i_d^+}{v_{Re}^0} \tag{65}$$

$$i_{Im}^0 = 0 \tag{66}$$

It can be seen from (63)-(66) that, reference currents contain only positive and zero sequence components under unbalanced grid conditions. The proposed control strategy helps in removing the oscillations in active and reactive power for a three-phase four-wire system. Furthermore, it also helps in reducing the current amplitude in the faulty phase.

The proposed strategy is advantageous in terms of power controllability, at the cost of increased computational burden due to two extra control objectives.

5) FLEXIBLE PEAK CURRENT LIMITING CONTROL (FPCLC) [110]

In [110], [111], a fully flexible current controller is proposed that limits the peak currents to improve the ride through services by injecting positive and negative components of the active and reactive powers, P^+, P^-, Q^+ and Q^-, respectively. The control scheme ensures that the injected currents do not surpass the inverter rated current and avoid overcurrent tripping of the PV inverter to guarantee its safe and reliable operation. The positive and negative sequence currents are derived in SRF as in (67)-(70).

$$I_p^+ = \frac{2}{3}\frac{P^+}{V^+} = \frac{2}{3}\frac{k_PP}{V^+} \tag{67}$$

$$I_p^- = \frac{2}{3}\frac{P^-}{V^-} = \frac{2}{3}\frac{(1-k_P)P}{V^-} \quad (68)$$

$$I_q^+ = \frac{2}{3}\frac{Q^+}{V^+} = \frac{2}{3}\frac{k_q Q}{V^+} \quad (69)$$

$$I_q^- = \frac{2}{3}\frac{Q^-}{V^-} = \frac{2}{3}\frac{(1-k_q)Q}{V^-} \quad (70)$$

From (67)-(70), there are four parameters P^+, P^-, Q^+, Q^-, and hence several combinations are possible to limit the peak currents. In [110], the relation among these variables is established and the control gains are defined as in (71)-(73).

$$k_P = \frac{P^+}{P} \quad \text{and } k_Q = \frac{Q^+}{Q} \quad (71)$$

$$P^+ = k_P P, \quad P^- = (1-k_P)P \quad (72)$$

$$Q^+ = k_Q Q, \quad Q^- = \left(1-k_Q\right)Q \quad (73)$$

where, $P = P^+ + P^-$ and $Q = Q^+ + Q^-$ and k_P and k_q are the active and reactive control gain, respectively.

It is observed that the phase currents I_a, I_b and I_c correspond to a unique solution of Q_a, Q_b and Q_c, respectively. The maximum value among the phase currents is then determined to ensure safe operation of the inverter as in (74).

$$Q_{min} = min\{Q_a, Q_b, Q_c\} \Rightarrow max\{I_a, I_b, I_c\} = I_{(max)} \quad (74)$$

A generalized expression is derived, to evaluate the reactive powers for each phase to limit the peak current as in (75)-(78).

$$Q = \frac{-2xP + \sqrt{y\left(3I_{(max)}nV^+\right)^2 - (2zP)^2}}{2y} \quad (75)$$

$$x = \left(k_P + k_q - 2k_P k_q\right) nsin\left(\hat{\varphi}\right) \quad (76)$$

$$y = k_q^2\left[1 + 2ncos\left(\hat{\varphi}\right) + n^2\right] - 2k_q\left[1 + ncos\left(\hat{\varphi}\right)\right] \quad (77)$$

$$z = k_P\left[1 - ncos\left(\hat{\varphi}\right)\right] + k_q\left[1 + ncos\left(\hat{\varphi}\right)\right] + k_P k_q\left[n^2 - 1\right] - 1 \quad (78)$$

And the different values for Q_a, Q_b and Q_C are obtained from the three distinct values of $\hat{\varphi}$ as in (79).

$$\hat{\varphi} = \left\{\varphi, \varphi + \frac{2}{3}\pi, \varphi - \frac{2}{3}\pi\right\} \quad (79)$$

The reactive power reference will be the minimum value among Q_a, Q_b and Q_C and once this reference is determined, the positive and negative sequence of active and reactive powers, i.e., P^+, P^-, Q^+ and Q^-, respectively can be known.

This strategy is advantageous in terms of its flexibility and capability to balance positive and negative components of the active and reactive power at the same time while restricting the currents to a safe value. It is applicable to all sizes of power converters having different ratings. But the major drawback of this strategy is its increased complexity as compared with other control schemes as it highly depends on the VUF and the phase angle between sequences which may have limited practical applications. Moreover, the proposed strategy does not provide zero active power oscillations.

6) PEAK CURRENT LIMIT CONTROL (PCLC) [112]

In [112], a strategy is proposed to avoid overcurrent protection by providing peak current limitation (PCL) of negative sequence current. To guarantee that the highest current does not exceed the pre-defined value (I_{max}), the maximum amplitude of the negative sequence current injection (I_{PCL}^-) is calculated as in (80).

$$I_{PCL}^- = -I^+\cos\left(\varphi + k\frac{4\pi}{3}\right) + I^{+2}[\cos^2(\varphi + k\frac{4\pi}{3}) - 1] + I_{max}^2$$

$$k = \left\{\begin{array}{ll} 0, & -\frac{\pi}{3} \geq \varphi < \frac{\pi}{3} \\ 1, & \frac{\pi}{3} \geq \varphi < \pi \\ -1, & \pi \geq \varphi < \frac{5\pi}{3} \end{array}\right\} \quad \text{and}$$

$$\varphi = \emptyset_n + \emptyset_p + \emptyset_1 - \emptyset_2 \quad (80)$$

Symbols have their usual meanings as in [108]. The injection of active and reactive current is flexible; hence the strategy is useful in satisfying the requirements of commonly available grid codes. Moreover, by injecting a specific combination of active and reactive currents, this method eliminates the ripples in active power.

7) LIMIT-THE-CURRENT CONTROL STRATEGY (LCCS) [113]

To overcome the drawback mentioned in [110], a control strategy is proposed in [113], which is independent of VUF and the phase angle. This strategy provides flexible control to ensure proper regulation in the injection of the power components and limits the current to avoid nuisance tripping of the inverters. The peak values of currents during normal and abnormal grid conditions are determined from (81) and (82), respectively.

$$I_{balanced}^* = \frac{2P^*}{3V^+} \quad (81)$$

$$I_{unbalanced}^* = \frac{2P^*}{3\left(V^+ - V^-\right)} \quad (82)$$

It can be seen from (81)-(82) that the presence of the negative sequence component under unbalance voltage condition results in higher peaks in current. Hence, minimization of these peaks in current by formulating the current references in the stationary reference frame is obtained as in (83)-(86).

$$i_{\alpha(p)}^* = \frac{2}{3}\frac{I_P^*\sqrt{\left(v_\alpha^+\right)^2 + \left(v_\beta^+\right)^2}}{\left[\left(v_\alpha^+\right)^2 + \left(v_\beta^+\right)^2\right] + k_p\left[\left(v_\alpha^-\right)^2 + \left(v_\beta^-\right)^2\right]} \times \left[\left(v_\alpha^+\right) + \left(k_p v_\alpha^-\right)\right] \quad (83)$$

$$i_{\beta(p)}^* = \frac{2}{3}\frac{I_P^*\sqrt{\left(v_\alpha^+\right)^2 + \left(v_\beta^+\right)^2}}{\left[\left(v_\alpha^+\right)^2 + \left(v_\beta^+\right)^2\right] + k_p\left[\left(v_\alpha^-\right)^2 + \left(v_\beta^-\right)^2\right]} \times \left[\left(v_\beta^+\right) + \left(k_p v_\beta^-\right)\right] \quad (84)$$

$$i^*_{\alpha(q)} = \frac{2}{3}\frac{I^*_q\sqrt{\left(u^+_\alpha\right)^2+\left(u^+_\beta\right)^2}}{\left[\left(v^+_\alpha\right)^2+\left(v^+_\beta\right)^2\right]+k_p\left[\left(v^-_\alpha\right)^2+\left(v^-_\beta\right)^2\right]} \times\left[\left(v^+_\beta\right)+\left(k_q v^-_\beta\right)\right] \tag{85}$$

$$i^*_{\beta(q)} = \frac{2}{3}\frac{I^*_q\sqrt{\left(u^+_\alpha\right)^2+\left(u^+_\beta\right)^2}}{\left[\left(v^+_\alpha\right)^2+\left(v^+_\beta\right)^2\right]+k_p\left[\left(v^-_\alpha\right)^2+\left(v^-_\beta\right)^2\right]} \times\left[\left(-v^+_\alpha\right)-\left(k_q v^-_\alpha\right)\right] \tag{86}$$

where, I^*_P and I^*_q denotes the active and reactive current references, respectively. The reference of the maximum current (I^*_{max}), in (83)-(86) is obtained from (87).

$$I^*_{max} = \frac{2}{3}\sqrt{\left[\frac{I^*_p\left(V^+\right)^2}{\left(V^+\right)^2+k_p\left(V^-\right)^2}\right]^2+\left[\frac{I^*_q\left(V^+\right)^2}{\left(V^+\right)^2+k_q\left(V^-\right)^2}\right]^2} + \frac{2}{3}\sqrt{\left[\frac{k_pI^*_pV^+V^-}{\left(V^+\right)^2+k_p\left(V^-\right)^2}\right]^2+\left[\frac{k_qI^*_qV^+V^-}{\left(V^+\right)^2+k_q\left(V^-\right)^2}\right]^2} \tag{87}$$

For different values of k_p and k_q, peak values of currents are obtained, and the proposed scheme reduces the current peaks under polluted grid conditions. The maximum value of current in (87) is determined from the active and reactive current references and the positive and negative sequence components of voltage at PCC. To ensure that the current stays within the permissible limit the current references are formulated in (88), where I_{rated} and I_{max} represents the rated current value of the inverter and the maximum among the three-phase currents, i.e., $I_{max} = \max\{I_a, I_b, I_c\}$, respectively.

$$\begin{bmatrix}\hat{i}^*_a\\ \hat{i}^*_b\\ \hat{i}^*_c\end{bmatrix} = \frac{I_{rated}}{I_{max}}\begin{bmatrix}\hat{i}^*_{\alpha(p)}+\hat{i}^*_{\alpha(q)}\\ -\left(\hat{i}^*_{\alpha(p)}+\hat{i}^*_{\alpha(q)}\right)/2+\sqrt{3}\left(\hat{i}^*_{\beta(p)}+\hat{i}^*_{\beta(q)}\right)/2\\ -\left(\hat{i}^*_{\alpha(p)}+\hat{i}^*_{\alpha(q)}\right)/2-\sqrt{3}\left(\hat{i}^*_{\beta(p)}+\hat{i}^*_{\beta(q)}\right)/2\end{bmatrix} \tag{88}$$

Here, $\hat{i}^*_a, \hat{i}^*_b, \hat{i}^*_c$ are the current references in the natural reference frame. The maximum value of the current reference in (88) is I_{rated} under severe grid fault. As compared to the control strategy in [110], this scheme is simpler as it is independent of the voltage unbalance factor and angle between component sequences which can provide flexible regulation in injected powers and limitation in current amplitudes to avoid overcurrent protection.

8) POSITIVE AND NEGATIVE SEQUENCE G AND B CONTROL (PNGBC) [114]

In [114], positive and negative sequence conductance (G) and susceptance (B) based control method is proposed to achieve multiple objectives like current limitation, minimization of oscillation in active and reactive powers as in (89)-(90).

$$g^- = k_G g^+ \tag{89}$$

$$b^- = k_B b^+ \tag{90}$$

where, k_G and k_B are the proportional ratio between positive sequence and negative sequence of G and B, respectively and g^+, g^-, b^+ and b^- are the positive and negative sequence components of susceptance and conductance, which are obtained using (91) and (92), respectively.

$$g^+ = \frac{2}{3}\frac{\mathrm{P}}{\left|\mathrm{v}^+\right|^2-k_G\left|\mathrm{v}^-\right|^2} \tag{91}$$

$$b^+ = \frac{2}{3}\frac{\mathrm{Q}}{\left|\mathrm{v}^+\right|^2-k_B\left|\mathrm{v}^-\right|^2} \tag{92}$$

where, k_G, k_B can take any values between -1 to 1. Once g^+ and b^+ are calculated (g^+_{cal}, b^+_{cal}), the current amplitude of each phase can be easily determined. Further, the maximum phase current (I_{max}) is calculated as in (93).

$$I_{max} = \max\left(I_{amp}, I_{bmp}, I_{cmp}\right) \tag{93}$$

where, I_{amp}, I_{bmp} and I_{cmp} are the current amplitude in phase a, b and c, respectively. Then the appropriate value of current is selected based on the converter capacity as I_{lim}. To avoid the operation of overcurrent protection devices the values of g^+ and b^+ are determined from (94)-(95), respectively.

$$g^+ = \begin{cases} g^+_{cal}, & I_{max} \le I_{lim} \\ \dfrac{I_{lim}}{I_{max}}g^+_{cal}, & I_{max} > I_{lim}\end{cases} \tag{94}$$

$$b^+ = \begin{cases} b^+_{cal}, & I_{max} \le I_{lim} \\ \dfrac{I_{lim}}{I_{max}}g^+_{cal}, & I_{max} > I_{lim}\end{cases} \tag{95}$$

If the maximum current I_{max} is less than I_{lim}, the overcurrent control is avoided. On the other hand, when I_{max} is greater than I_{lim}, the current is proportionally decreased based on the ratio of (I_{lim}/I_{max}) and thus prevents overcurrent with the maximum phase current being limited to I_{lim}.

9) SINUSOIDAL CURRENT INJECTION STRATEGY (SCIS) [115]

A control strategy that eliminates the double grid frequency oscillation in active power and dc-link voltage with the capability of injecting sinusoidal current is proposed in [115]–[117]. The strategy formulates flexible active and reactive current references, based on PNSC strategy, under unbalanced fault. It also limits the injected current to the rated value during faults. Moreover, this scheme involves a non MPPT operating mode under severe faults when the maximum power from the PV array results in overcurrent in the inverter.

The reference currents are formulated in the stationary reference frame by taking four key parameters $k_{\alpha p}$, $k_{\beta p}$, $k_{\alpha q}$ and $k_{\beta q}$ (96)-(99).

$$i_{\alpha P} = \frac{v_\alpha^+ - v_\alpha^-}{\left(v_\alpha^{+^2} + v_\beta^{+^2}\right) + k_{\alpha P}(90\left(v_\alpha^{-^2} + v_\beta^{-^2}\right)} P^* \quad (96)$$

$$i_{\beta P} = \frac{v_\beta^+ - v_\beta^-}{\left(v_\alpha^{+^2} + v_\beta^{+^2}\right) + k_{\beta P}\left(v_\alpha^{-^2} + v_\beta^{-^2}\right)} P^* \quad (97)$$

$$i_{\alpha Q} = -\frac{v_{\alpha\perp}^+ + v_{\alpha\perp}^-}{\left(v_{\alpha\perp}^{+^2} + v_{\beta\perp}^{+^2}\right) + k_{\alpha Q}\left(v_{\alpha\perp}^{-^2} + v_{\beta\perp}^{-^2}\right)} Q^* \quad (98)$$

$$i_{\beta Q} = -\frac{v_{\beta\perp}^+ + v_{\beta\perp}^-}{\left(v_{\alpha\perp}^{+^2} + v_{\beta\perp}^{+^2}\right) + k_{\beta Q}\left(v_{\alpha\perp}^{-^2} + v_{\beta\perp}^{-^2}\right)} Q^* \quad (99)$$

where, P^* is obtained from the dc-link voltage control loop and Q^* is the required reactive power during fault condition. The values of these parameters in (96)-(99) are chosen either +1 or -1 to modify the active and reactive current references according to grid specifications as in Table 4. As evident from (96)-(99), the use of mode 2 is suggested, to utilize the inverter's rated capacity.

TABLE 4. Different modes for utilizing inverter's rated capacity.

Mode	$k_{\alpha P}$	$k_{\beta P}$	$k_{\alpha Q}$	$k_{\beta Q}$
1	+1	+1	+1	+1
2	−1	−1	−1	−1
3	+1	+1	−1	−1
4	−1	−1	+1	+1

Once the voltage sag occurs, the controller determines the inverter pseudo power, namely, the new nominal power (NNP) of the inverter which is determined by the voltage sag depth. The NNP is evaluated as in (100).

$$\text{NNP} = \frac{\sqrt{V_p} - \sqrt{V_n}}{V_{base}} S \quad (100)$$

where, the nominal power is denoted by S, V_{base} is the base voltage and it is equal to the RMS value of line-line grid voltage, $V_p = v_\alpha^{+^2} + v_\beta^{+^2}$ and $V_n = v_\alpha^{-^2} + v_\beta^{-^2}$. Based on the per-unit depth in voltage sag, the reactive power is calculated as per the Chinese grid code as in (101).

$$\begin{cases} Q = 0, & if\ V_{pu} > 0.9 \\ Q = S \times 1.5 \times \left(0.9 - V_{pu}\right), & if\ 0.2 < V_{pu} < 0.9 \\ Q = 1.05 \times S, & if\ V_{pu} < 0.2 \end{cases} \quad (101)$$

where, $V_{pu} = \frac{\sqrt{v_\alpha^2 + v_\beta^2}}{V_b}$. To avoid overcurrent, the new reference power (P_{max}) to be injected into the grid is $P_{max} = \sqrt{NNP^2 - Q^2}$. Under severe faults, if ($Q > NNP$), Q is selected as NNP, and the reference power P_{max} is taken as 0, which means only reactive power is injected. This is because of the low nominal power of the inverter and is not capable of delivering active power to the grid to avoid overcurrent. However, the control strategy allows double grid frequency oscillations within the reactive power. Moreover, the smooth transition from MPPT to de-rated MPPT is not achieved [118]. To remove these oscillations in reactive power, under normal and abnormal grid conditions for a low voltage distribution grid, a robust Kalman filter (RKF) is employed in [119]. A smooth transition from MPPT to de-rated MPPT is achieved with the help of this strategy.

The function of RKF is to calculate the magnitude of the fundamental load component (FLC) from the load current, which enhances the system dynamics under load perturbation. The KF is the mathematical approach, which works through a prediction and correction module.

10) MULTI-OBJECTIVE CONTROL STRATEGY (MOCS) [120]

In [120], the control algorithm simultaneously mitigates the challenges associated with power quality and provides overcurrent limitation. To achieve the control objectives, current references are formulated in the stationary reference frame as given in (102)-(103) [96].

$$I_\alpha^* = \frac{2}{3}\left(\left(\frac{\left(k_p^+ v_\alpha^+ + k_p^- v_\alpha^-\right) P^*}{k_p^+ \left(V^+\right)^2 + k_p^- \left(V^-\right)^2}\right) + \left(\frac{\left(k_q^+ v_\beta^+ + k_q^- v_\beta^-\right) Q^*}{k_q^+ \left(V^+\right)^2 + k_q^- \left(V^-\right)^2}\right)\right) \quad (102)$$

$$I_\beta^* = \frac{2}{3}\left(\left(\frac{\left(k_p^+ v_\beta^+ + k_p^- v_\beta^-\right) P^*}{k_p^+ \left(V^+\right)^2 + k_p^- \left(V^-\right)^2}\right) - \left(\frac{\left(k_q^+ v_\alpha^+ + k_q^- v_\alpha^-\right) Q^*}{k_q^+ \left(V^+\right)^2 + k_q^- \left(V^-\right)^2}\right)\right) \quad (103)$$

where, k_p^+, k_p^-, k_q^+ and k_q^- are the four variable parameters. P^* and Q^* are the active power and reactive power references, respectively. By using (102) and (103), the injected reference current can be determined from the positive and negative-sequence components of the active and reactive currents (I_p^+,I_p^-, I_q^+ and I_q^-), respectively. The current amplitude in each phase is determined as in (104)-(106), as shown at the bottom of the next page.

The maximum values of the phase current (I_{max}) is evaluated using (107).

$$I_{max} = \sqrt{\frac{\left(V^+\right)^2 - 2V^+V^-x + \left(V^-\right)^2}{\left(V^+\right)^2}\left(\left(I_p^+\right)^2 + \left(I_q^+\right)^2\right)} \quad (107)$$

where, $x = min\left\{cos\left(\theta\right), cos\left(\theta - \frac{2\pi}{3}\right), cos\left(\theta + \frac{2\pi}{3}\right)\right\}$. It can be observed from (107), that the minimum value of x results in the maximum value of phase currents. To protect

the inverter against overcurrent,

$$I_{max} \leq I_{rated} \tag{108}$$

By using (107) and (108) current limitation is guaranteed. By substituting the value of $I_p^+ = I_{p\,max}^+$ and $I_{max} = I_{rated}$ in (107), the maximum active current ($I_{p\,max}^+$) is obtained as in (109).

$$I_{p\,max}^+ = \sqrt{\frac{\left(V^+\right)^2 (I_{rated})^2}{\left(V^+\right)^2 - 2V^+V^-x + \left(V^-\right)^2} - \left(I_{qGC}^+\right)^2} \tag{109}$$

where, I_{qGC}^+ represents the positive sequence reactive current, which is defined by the grid code during voltage sag. Under LVRT condition, to prioritize the injection of reactive power the value of I_p^+ is always less than I_{pmax}^+.

However, in the case of low-power production, if I_p^+ is less than the $I_{p\,max}^+$, the rated current capacity of the inverter is not fully utilized. Therefore, the amplitude of the reference reactive current is increased to fully utilize the current capacity of the inverter to provide maximum voltage support. By substituting $I_{max} = I_{rated}$ in (107), I_q^+ is determined as in (110).

$$I_q^+ = \sqrt{\frac{\left(V^+\right)^2 (I_{rated})^2}{\left(V^+\right)^2 - 2V^+V^-x + \left(V^-\right)^2} - \left(I_p^+\right)^2} \tag{110}$$

11) PEAK CURRENT CONTROL WITH RESCALING FACTOR (PCCRF) [121]

In [121], zero oscillations in active power are achieved at the expense of higher peak currents in one or two phases. Hence, to limit these currents, a rescaling factor (k_{rs}) is used to formulate the current references as in (111).

$$k_{rs} = \begin{cases} \dfrac{I_{rms}}{I_{rms-max}^*}, & if\ I_{rms-max}^* > 1 \\ 1, & if\ I_{rms-max}^* \leq 1 \end{cases} \tag{111}$$

where, I_{rms} is the rms value of the nominal current of the inverter and $I_{rms-max}^*$ is the maximum rms value of the three-phase current references.

The current references are determined as in (112).

$$\begin{bmatrix} \bar{i}_a^* \\ \bar{i}_b^* \\ \bar{i}_c^* \end{bmatrix} = k_{rs} \begin{bmatrix} i_a^* \\ i_b^* \\ i_c^* \end{bmatrix} \tag{112}$$

where, $\bar{i}_a^*$, $\bar{i}_b^*$ and $\bar{i}_c^*$ are the current references in natural reference frame, after rescaling. The error and the instantaneous phase current are then tracked using the proportional (PR) controller and the voltage references are generated in stationary ($\alpha\beta$) reference frame.

12) OVER CURRENT CONTROL IN DISTRIBUTED GENERATION SYSTEMS (OCCIDGS) [99]

A strategy to limit the maximum inverter current to avoid overcurrent protection is proposed in [99]. The strategy determines the maximum safe current of the inverter based on the minimum value of the angles among the three phases as in (113).

$$\mathrm{I_{max}} = \sqrt{1 - 2nx + n^2}\sqrt{\left(I_p^+\right)^2 + \left(I_q^+\right)^2} \tag{113}$$

where, n is the voltage unbalance factor. Also $x = \min\left\{\cos(\emptyset), \cos\left(\emptyset - \frac{2}{3}\pi\right), \cos\left(\emptyset + \frac{2}{3}\pi\right)\right\}$

The proposed strategy also provides maximum voltage support by ensuring that the current injection is based on the chosen injection angle θ_{inj}, for which the amplitudes of the positive-sequence currents i_p^+ and i_q^+ is defined as in (114) and (115), respectively.

$$i_p^+ = i_{p(opt)}^+ = I\cos\theta_{inj} \tag{114}$$

$$i_q^+ = i_{q(opt)}^+ = I\cos\theta_{inj} \tag{115}$$

where,

$$I = \frac{\mathrm{I_{rated}}}{\sqrt{1 - 2nx + n^2}} \tag{116}$$

Apart from the above-mentioned strategies, several other improvements have been proposed to provide current limitation under unbalanced grid voltage conditions. A current reference generation strategy is proposed in compliance with the recently developed grid codes (CRGGC) in which the positive and negative sequence reactive currents are injected in proportion with the change in positive and negative sequence

$$I_a = \sqrt{\frac{\left(V^+\right)^2 - 2V^+V^-\cos(\theta) + \left(V^-\right)^2}{\left(V^+\right)^2}\left(\left(I_p^+\right)^2 + \left(I_q^+\right)^2\right)} \tag{104}$$

$$I_b = \sqrt{\frac{\left(V^+\right)^2 - 2V^+V^-\cos\left(\theta - \frac{2\pi}{3}\right) + \left(V^-\right)^2}{\left(V^+\right)^2}\left(\left(I_p^+\right)^2 + \left(I_q^+\right)^2\right)} \tag{105}$$

$$I_c = \sqrt{\frac{\left(V^+\right)^2 - 2V^+V^-\cos\left(\theta + \frac{2\pi}{3}\right) + \left(V^-\right)^2}{\left(V^+\right)^2}\left(\left(I_p^+\right)^2 + \left(I_q^+\right)^2\right)} \tag{106}$$

voltage [122]. The distribution factors used in the strategy for active power reference and reactive power reference are designed explicitly in accordance with the modern grid codes. The proposed strategy utilizes the converter's full capacity, avoids overvoltage at the PCC, and reduces the unbalance factor. In [123], another strategy is proposed that maximizes the power delivery and provides current limitation. The strategy employs a DDSRF to extract the positive and negative sequence of voltages and currents. The proposed DDSRF based PNS extractor exhibits faster response and lower total harmonic distortion (THD) compared to other techniques. In [124], a CRG scheme is proposed which minimizes the oscillations in active and reactive powers. A FOPI (Fractional-order PI) controller instead of the conventional PI, PR controllers, is employed to obtain the zero steady-state error in the stationary reference frame which improves the response time. In [125], [126], a control strategy is proposed that helps in maximizing the power capability of PV inverter. The flexible current injection strategy is developed by ensuring a proper balance between positive and negative sequence components. The strategy limits the current to its rated value and avoids the oscillations in active power. Table 5 presents a comparison of recently developed current limitation strategies, based on their distinct characteristics.

IV. DC-LINK VOLTAGE CONTROL

The design of an efficient dc-link voltage control loop is essential during LVRT operation. Under normal operating conditions, the power extracted from the PV array is delivered to the grid through a dc-link capacitor to ensure that the power balance is achieved. It is well-known, that the reactive power reference during LVRT under faulty grid conditions is determined from the grid codes, whereas the active power reference is dependent on the inverter power rating. The injected active power to the grid (P_{inj}), should follow the reference power (P^*) when there is no sag present, i.e., when $P^* \geq P_{inj}$. The power imbalance occurs in the system when there is inequality between the reference power (P^*) and the injected active power. This usually occurs under unbalanced voltage sag conditions, as the inverter capacity is mostly utilized to inject reactive power, and the MPP power from the PV array cannot be fed to the grid. To overcome this, the MPPT is terminated as the active power injection capability of the inverter is now reduced. If the MPPT is still operating, the power imbalance may give rise to overvoltage across the dc-link capacitor that may result in the deterioration of the capacitor and thus reduce its life. To safeguard the dc-link capacitor from overvoltage, a constant dc-link voltage is achieved, and power balance is ensured by active power curtailment. This is done by reducing the power extracted from the PV array by shifting the point of operation away from the MPP on the P-V curve to a new reduced reference power operating point [127]. Single-stage GCPV systems are self-protected as the operating point shifts to a new point in the I-V curve to curtail down the active power under voltage sag conditions [128]. Nevertheless, in two-stage systems, the MPPT operation is performed by dc-dc converter [129], hence, the system is not self-protected. A separate control loop is required to protect the over voltages in the dc-link capacitor. The response of constant dc-link voltage control strategy under unbalanced and balanced grid faults are shown in Figure 8 (a) and (b), respectively.

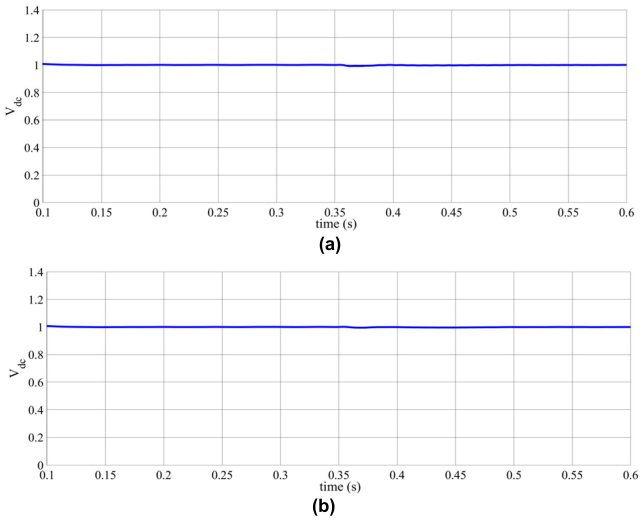

FIGURE 8. Response of dc-link voltage control strategy in pu across dc-link capacitor under (a) unbalanced and (b) balanced grid faults.

On the other hand, there are several challenges associated with providing a constant dc-link voltage under unbalanced sag conditions [130]–[132]. Under deep grid voltage sag conditions, a constant dc-link voltage results in the injection of non-sinusoidal unbalanced currents which is due to a low modulation index [133].

It is well-known that if a fixed reference value of the dc-link voltage is chosen for the worst condition, it results in high switching and inductor losses in two-stage PV systems [134]. In [135], an adaptive dc-link voltage technique is suggested that shows that the PV system may have an increase in the lifetime of 75.76% as compared to the fixed dc-link control strategy. Hence, there exists a trade-off when operating the dc-link capacitor at a fixed or variable voltage. Therefore, the dc-link voltage control strategies are classified into two sub-sections, namely constant and adaptive dc-link voltage control. This paper focuses on discussing the recently developed dc-link voltage control strategies for two-stage PV systems to limit the scope of the proposed study.

A. CONSTANT DC-LINK VOLTAGE CONTROL

This section discusses the recently developed control strategies, to maintain a constant dc-link voltage. These methods mitigate the double grid frequency oscillations within the dc-link voltage with improved dynamic response during fault conditions.

1) INJECTION OF LESS POWER DURING SAG (ILPDS) [127]

In [127], three solutions are suggested to limit the dc-link overvoltage by reducing the active power from:

TABLE 5. Comparison between current limitation strategies under low-voltage-ride-through condition.

Reference, Strategy	Controller	Experimental results	Advantages	Disadvantages	THD	Efficiency	Accuracy	Power Factor	Network Losses	Dynamic Response
[99], OCCIDGS	PR	Yes	• Reduced voltage imbalance	• Large oscillations in reactive power during unbalanced grid faults	Low	High	High	High	Low	Excellent
[106], TDPC	PR	Yes	• Reduction in inverter overcurrent	• No regulation on the minimum set point in the reduction of inverter overcurrent • High THD in current under unbalanced grid voltage	High	Low	High	Low	Low	Poor
[107], MPGICC	PR	Yes	• Guarantees minimum peak value in inverter current	• Only reactive power injection is considered • High THD	High	High	Low	Low	Low	Excellent
[108], RROCP	PR	Yes	• Improved efficiency • Reduction in input current ripples	• High overshoot in current • Sustained oscillations in active and reactive powers	Low	High	Low	High	Low	Excellent
[109], ZSCC	PI, PR, HC	No	• Enhanced power controllability • Use of zero sequence component to mitigate oscillations in active and reactive powers	• Increased computational burden • Effects of unbalanced faults are not considered on constant dc-link voltage	Low	High	High	High	Low	Poor
[110], FPCLC	PR	Yes	• Improved LVRT services by limiting the currents under a safe value • Capability to balance positive and negative components of the active and reactive power at the same time • Applicable to all size of power converters	• Dependent on VUF • High complexity • Large oscillations in the injected power components	Low	Low	Low	High	High	Poor
[112], PCLC	PR	Yes	• Reduced second harmonic ripples in the dc-link voltage • Peak currents are limited	• Sustained oscillations in active and reactive power	High	Low	High	Low	Low	Excellent
[113], LCCS	PR	Yes	• Independent of VUF • Flexible power control	• Since the preference is given to current limitation, active and reactive powers require some specific values of K_p and K_i to match the reference power	Low	High	low	High	Low	Poor
[114], PNGBC	PR	Yes	• Minimizes the oscillations in active and reactive powers	• Application is limited to high power ratings • Applicable mainly for inductive grids	Low	High	Low	High	Low	Excellent
[115], SCIS	PR	Yes	• Oscillations in active power are minimized	• Large oscillations in reactive power	Low	High	High	Low	High	Excellent
[120], MOCS	PR	Yes	• Oscillations in real power are removed • Control algorithm is based on power management strategy	• Poor dynamic performance • Only the positive-sequence reactive current is regulated to comply with grid codes	Low	High	Low	High	High	Excellent
[121], PCCRF	PR	Yes	• Maximum capability of inverter is exploited • Zero active power oscillations	• Oscillations in active power • Unbalanced injected currents	High	High	Low	Low	High	Excellent
[122], CRGCC	PR, DSRF	Yes	• Overvoltage at the PCC is avoided • Current limitation is achieved in compliance with the next generation grid codes	• Oscillations in active and reactive power under unbalanced faults	Low	High	Poor	High	High	Excellent
[123], MPDIDG	PI, DDSRF	No	• Improved P and Q controllability • Low THD in the injected currents • Reduced oscillations in P and Q	• Control strategy is not as per any specific grid code • Reactive power compensation issues are not addressed	High	High	High	Low	Low	Excellent
[124], FCCIDG	Fractional order PI (FOPI)	No	• Zero steady-state error with the help of FOPI controller • Fast response time and robustness under grid faults • Reduced oscillations in active and reactive power	• Poor power control due to lack of power management strategy • No voltage support at the PCC	Low	High	Low	Low	Low	Excellent

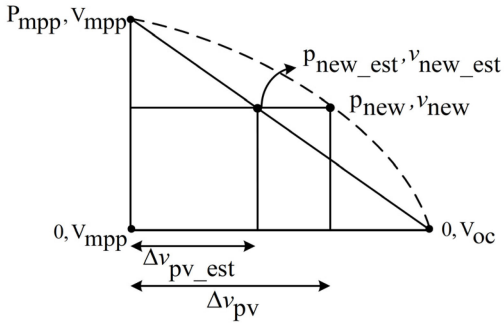

FIGURE 9. Approximation of new operating point.

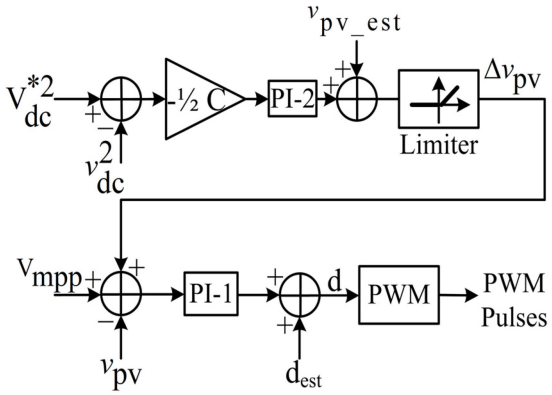

FIGURE 10. Controller to obtain non-MPP operating point.

Short-circuiting the PV (P = 0), Open-circuiting the PV (P = 0) and extracting non-MPP power from the PV array (P ≠ 0). In the first two methods, no power is extracted from the PV array, hence, only reactive power is injected into the grid. However, in the third method, less power, as compared to the pre-fault MPP power, is injected into the grid by controlling the dc-dc converter. The controlling of the dc-dc converter is done in such a way that the power generated by the PV array matches the injected power to the grid. The operating point moves to a new point to obtain power balance. To ensure that the point of operation moves to the right-side of MPP on the P-V curve, a positive voltage step Δv_{pv} is added to v_{mpp} as in (117).

$$v_{new} = v_{mpp} + \Delta v_{pv} \tag{117}$$

Faster dynamics are obtained by regulating the energy stored in the dc-link capacitor ($\frac{1}{2}CV_{dc}^2$). In Figure 9, p_{new_est}, v_{new_est} are the estimated power and voltage in the triangle, respectively. From Figure 9, v_{new_est} can be evaluated as in (118).

$$v_{new\_est} = \frac{p_{new\_est}}{P_{mpp}} \left(v_{mpp} - v_{oc}\right) + v_{oc} \tag{118}$$

where, p_{mpp} and v_{mpp} are the power and voltage at MPP, respectively before the fault. The new estimated power, p_{new_est} is evaluated from the active current reference as in (119).

$$p_{new\_est} \sim p_{out} = e_d i_{dref} \tag{119}$$

Simplifying (115) and (117), the new operating point and the voltage difference between the MPP and the new operating can be estimated using (120) and (121), respectively.

$$v_{new\_est} = \frac{e_d i_{dref}}{P_{mpp}} \left(v_{mpp} - v_{oc}\right) + v_{oc} \tag{120}$$

and

$$\Delta v_{pv\_est} = v_{new\_est} - v_{mpp} \tag{121}$$

The Δv_{pv_est} in (120) is added to the feedforward controller before the limiter as in Figure 10. The limiter gives the positive values for Δv_{pv} to obtain the v_{new} on the right-side of the PV curve. Moreover, the estimation of duty cycle (d_{est}) is determined as in (122).

$$d_{est} = 1 - \frac{v_{new_{est}}}{v_{dc}^*} \tag{122}$$

This scheme helps in injecting reduced power to the dc-link capacitor by moving the point of operation away from the MPP of the PV curve and has the advantage of injecting balanced currents even under faulty grid conditions.

2) FEEDBACK LINEARIZING CONTROL WITH SLIDING MODE COMPENSATION (FLCSMC) [136]

Several strategies have been proposed that use feedback linearizing control (FLC) in GCPV systems. However, the performance of FLC has not been investigated during the non-MPP mode of operation during grid faults. In [136], a robust FLC strategy is used, which employs sliding mode control to deal with the uncertainties during low-voltage-ride-through in GCPV systems. The proposed strategy controls the active and reactive power under LVRT and maintains a constant dc-link voltage.

In the case of asymmetrical grid conditions, FLC controls the active and reactive power to fulfill all the LVRT requirements and ensures constant dc-link voltage. The active and reactive power references are given as in (123).

$$\begin{cases} P^* = |s| \sqrt{1 - I_r^{*2}} \\ Q^* = |s| \, I_r^* \end{cases} \tag{123}$$

where, S is rated apparent power of the grid. To provide voltage support to the grid I_r^* is the injected reactive current as per the grid code.

In this mode, the power regulation is done to track reference trajectories given in (123). The proposed feedback sliding control is given as in (124).

$$i_\circ^* = C(-k_v e_v + \dot{v}_{dc}^* - \frac{\alpha_v}{C} sgn\,(s_v))) \tag{124}$$

where, k_v is the positive control gain, e_v denotes the tracking error, α_v is the sliding gain and s_v represents the sliding

surface for dc-link voltage control as in (125).

$$s_v = e_v(t) + k_v \int_0^t e_v(\tau)\, d\tau \tag{125}$$

The proposed controller results in a constant dc-link voltage when subjected to external disturbances like irradiance. This is because of the compensation provided by the sliding control within the feedback system. Hence, the proposed controller is superior to a conventional PI controller, which requires its control gains to be adjusted for all the uncertainties to achieve proper tuning.

3) NON-MPPT ALGORITHM WITH MCPC CONTROL (NMMCPCC) [137]

In [137], the hybrid control strategy is a combination of model current predictive control (MCPC) algorithm along with a non-MPPT algorithm. The MCPC algorithm minimizes the overcurrent in GCPV inverter and injects symmetrical currents even under faults. To eliminate the dc-link overvoltage problem, the non-MPPT algorithm evaluates the adjusted power for the PV array and a new duty cycle is acquired. The revised duty cycle is then used by the converter controller for proper tuning the output of PV array.

To alleviate the double grid frequency oscillations in dc-link voltage, a feedforward compensation is incorporated. The control diagram for non-MPPT mode is in Figure 11.

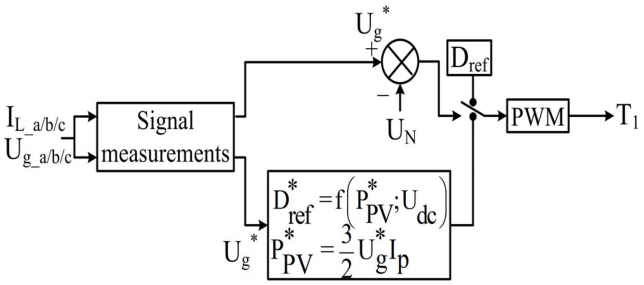

FIGURE 11. Control diagram for non-MPPT mode.

In non-MPPT mode, the duty ratio under the fault condition ($U_g^* < U_N$), is obtained as in (126).

$$D_{ref}^* = D + \left[U_{PV} - U_{ref}^*\right]\left(k_p + \frac{k_i}{s}\right) + \left(U_{DC} - U_{DC\_ref}\right) \times \left(k_{p\_dc}\frac{k_{i\_dc}}{s}\right) \tag{126}$$

where, U_{DC} denotes the dc-link voltage and U_{ref}^* is the reference voltage of non-MPPT mode. U_{ref}^* is obtained by the following set of equations given in (127).

Here, the fault voltages in the d-q frame of reference are represented by U_{gd}^*, U_{gq}^*.

$$\begin{cases} P_{PV}^* = AU_{ref}^* I_{SC}\left[1 - C_1\left(e^{\frac{U_{ref}^*}{(MC_2U_{OC})}} - 1\right)\right] \\ P_{PV}^* = 1.5U_g^*\sqrt{I_N^2 - I_{q_{set}}^2} \\ U_g^* = \sqrt{\left(U_{gd}^*\right)^2 + \left(U_{gq}^*\right)^2} \\ A = N\dfrac{S}{S_{ref}}\left[1 + \alpha\left(t - t_{ref}\right)\right] \end{cases} \tag{127}$$

In comparison to the conventional dual-loop control (outer voltage control loop and inner current control loop), this scheme eliminates the use of inner loop PI controller, PWM module and sequence separation techniques which result in balanced injected currents even under unbalanced fault conditions. The dc-link voltage is maintained at a constant level and double harmonics components are removed by using feedforward compensation.

Several other controllers have been proposed that help in maintaining a constant dc-link voltage [138]–[140]. By using the power references in (123) a constant dc-link voltage strategy is proposed in [141]. The strategy for PV inverter is developed based on a robust model predictive control. To achieve robustness, a disturbance compensator is employed in the system, which alleviates the tracking errors in the steady-state. In [142], an improved dynamic voltage regulation (IDVR) method is proposed to regulate the dc-link voltage with the help of a sliding mode controller along with a disturbance observer (SMC + DOB) in dc microgrids. The SMC ensures that the dc-link voltage is kept constant even in the presence of uncertainties and disturbances. To remove the chattering problem due to SMC, a saturation function is employed in place of the signum function. The use of an observer for the dc-link current helped in reducing the cost by removing the dc current sensor which helped in improving the reliability of the controller. In [143], a particle swarm optimization (PSO) based dc-link voltage control of a two-stage PV is proposed. A PI controller is employed to maintain the constant dc-link voltage and the parameters of this PI controller are obtained with the help of the optimization technique which helps in improving the dynamic response of the dc-link voltage. Another metaheuristic approach, namely the whale optimization technique (WOADCVC) is proposed in [144] for optimum tuning of the dc-link PI controller. It was reported that among other meta-heuristic approaches whale optimization algorithm (WOA) is best for tuning the PI controller.

B. ADAPTIVE DC-LINK VOLTAGE CONTROL

Although a constant dc-link voltage helps in enhancing the life of the dc-link capacitor, a variable dc-link voltage controller can assist in maintaining the modulation index within a certain range. By efficiently controlling the modulation index, high-quality current can be injected into the grid. An adaptive dc-link voltage control can also help in injecting more power as compared to a constant dc-link

voltage controller. This section discusses the recently developed control methods that adaptively vary the dc-link voltage.

1) VOLTAGE DROP RATIO BASED CONTROL (VDRBC) [145]

In [145], an adaptive dc-link voltage control method is formulated by ensuring that the inverter operates at a high modulation index in the linear region. The use of high modulation index helps in the injection of sinusoidal balanced currents into the grid which improves the output power quality. Under normal operating conditions, using the conventional control strategy, the dc-link voltage is fixed at a constant value. However, even under balanced voltage sag conditions, the proposed strategy follows the variable dc-link voltage reference (V'_{dc}), unlike the conventional strategy in which the dc-link voltage reference is fixed at a constant value. The variation in the update dc-link voltage reference V'_{dc} is dependent on the voltage dip as expressed in (128).

$$V_{pv} \leq V'_{dc} = \lambda * V^*_{dc} \tag{128}$$

where, V^*_{dc} is the reference value for the dc-link voltage control and λ is the voltage drop ratio tracked by the PLL. Further, the dc-link capacitor voltage is controlled by regulating the input and output current of the capacitor as in (129).

$$U = \frac{\left(\int (i_i - i_o)\, dt\right)}{C} \tag{129}$$

where, i_i is the input current to the capacitor and i_o is the output current. It is worth noting that the output current in (129) is fixed to avoid the nuisance tripping of the inverter. Hence, the current regulation is achieved by the input current.

As mentioned earlier, this strategy controls the dc-link voltage which ensures a high modulation index. However, under asymmetrical voltage sag conditions, the modulation index can be in the over modulation region, especially when the dc-link voltage reduces below a certain value. Hence, the operation in the over modulation is avoided by checking the maximum voltage difference between any two phases. Unlike the symmetrical voltage drop, double grid frequency oscillations occur in the case of unsymmetrical voltage drop. Therefore, under two-phase voltage drop conditions, the maximum and minimum values of the dc-link voltage are calculated as in (130).

$$v_a = V_1 sin\, \omega t \quad \text{and } v_b = V_2 sin\, (\omega t + 2\pi/3) \tag{130}$$

where, V_1 and V_2 in (128) denote the peak values of output voltages.

The maximum phase difference between phase A and phase B is given by (131), and the minimum value of the dc-link voltage to avoid over modulation can be determined using (132). The circuit diagram of the adaptive dc-link voltage controller is shown in Figure 12. The strategy is applicable for both, balanced and unbalanced grid voltage conditions and a well-designed PIR controller is used for the dc-link voltage control loop.

$$max\, (v_a - v_b) = \sqrt{V_1^2 + V_2^2 + V_1 V_2} \tag{131}$$

$$V_{dcmin} = 0.866\sqrt{V_1^2 + V_2^2 + V_1 V_2} \tag{132}$$

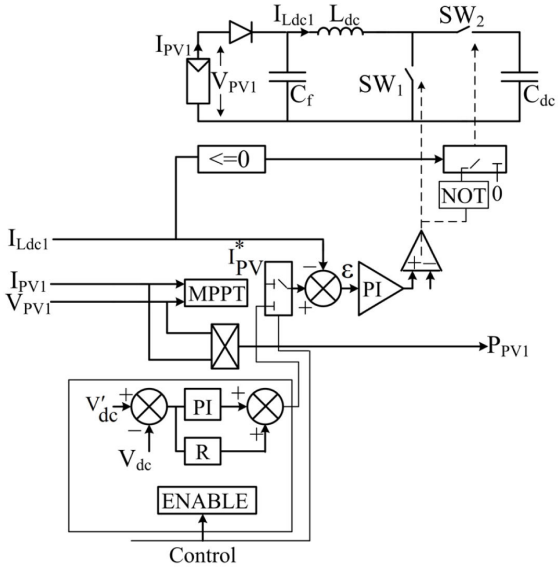

FIGURE 12. Adaptive dc-link voltage controller.

2) INTERWEAVED DFSOGI CONTROL (IDFSOGI) [146]

In [146], the dc-link voltage is adjusted with respect to the variations in PCC voltage. This adjustable dc-link voltage controller: minimizes the switching losses in the power converter devices, helps in reducing high frequency I^2R losses in the inductor and results in the reduction of ripple current. The reference duty ratio of the converter is evaluated as in (133).

$$D_{ref}\,(k) = 1 - \frac{V_{PVref}\,(k)}{V_{DC}\,(k)} \tag{133}$$

The reference dc-link voltage is determined using (134).

$$V_{DCref} = \mu\sqrt{3}V_Z \tag{134}$$

where $V_Z = \sqrt{\frac{2(v_{sa}^2+v_{sa}^2+v_{sa}^2)}{3}}$, is the phase voltage amplitude.

For an appropriate control action, the dc-link voltage must be about 10% greater than the voltage at the PCC. Hence, in (134) the value of μ is considered as 1.1. Switching losses in the inverter and the boost converter are dependent on the dc-link voltage, hence by keeping the dc-link voltage variable, these losses can be minimized.

The total energy loss (E) is obtained as in (135). Here, $P_{switch\,on}$, $P_{switch\,off}$ are the instantaneous power loss, when switch is on and off, respectively and t_{on}, t_{off} the total on-time and off-time, respectively.

$$E = \int_0^{t_{on}} P_{switch\,on} dt + P_{switch\,off}\, dt = \frac{1}{6} V_{DC} I_{VSC}\, \left(t_{on} + t_{off}\right) \tag{135}$$

The advantage of variable dc-link voltage is the minimization of high frequency ripple current in the inductor. The ripple current is expressed as in (136).

$$\Delta I \propto (V_s - V_{DC}) \tag{136}$$

It can be seen in (136), that the ripple current is dependent on the difference of instantaneous PCC line voltage (V_s) and

dc-link voltage (V_{DC}). The fixed dc-link voltage produces higher ripples in inductor current. As a result, the grid current is also influenced by these ripple currents.

By keeping the dc-link voltage close to the grid line voltage, these ripple currents can be reduced. With the help of the proposed strategy, more power is fed to the grid as compared to the injection of less power using the conventional control strategy with fixed dc-link voltage. The controller also results in a low THD of less than 5% in the presence of nonlinear load.

3) CPI BASED DC-LINK VOLTAGE CONTROL (CPIDCVC) [147]

It is clear now that the switching losses are dependent on the value of the dc-link voltage. In the case of fixed dc-link voltage, the switching losses are higher under both, normal and unbalanced grid conditions. Hence, another adaptive dc-link voltage control strategy is proposed in [147]. This strategy reduces the switching losses by adaptively changing the reference dc-link voltage with respect to the PCC voltage. The reference value of the dc-link voltage is obtained as in (137).

$$V_{DCref} = \tau V_{pcc}, \quad \text{where } \tau > 1 \tag{137}$$

To ensure that dc-link voltage remains higher as compared to the PCC voltage, the value of τ is taken as 1.1 as in [146].

Another strategy is proposed in [135] which reduces the dc-link voltage to its minimum possible value to inject more power into the grid. To avoid the operation of the inverter in over modulation region, a linearization strategy is employed which helps in improving the transient and dynamic performance of the system. In [148], another attractive approach is presented, in which an adaptive PI controller is used to obtain different control targets like stability, dynamic response, disturbance rejection and low overshoot. In this scheme, the control gains of the PI controller are adjusted adaptively by employing an anti-wind-up scheme, which effectively reduces the transients in the dc-link voltage. A comparative table on the above-mentioned dc-link voltage control strategies is prepared, based on their distinct characteristics as in Table 6.

V. OTHER MISCELLANEOUS CONTROL STRATEGIES

Apart from the above-discussed control strategies, few additional challenges exist that are addressed by the following control strategies.

A. VOLTAGE COMPENSATION CALCULATION CONTROL STRATEGY (VCCCS)

In [149], a multi-objective strategy implemented in the d-q reference frame is formulated. The strategy performs well under symmetrical and asymmetrical grid voltage conditions. It helps in generating sinusoidal voltage and currents and alleviating the need for a switch for a transition from MPPT to non-MPPT mode. Inverter currents are limited by adjusting the reference dc-link voltage (V_{dc}^*), thereby utilizing the positive sequence of d component. The q-component is utilized to supply the reactive power.

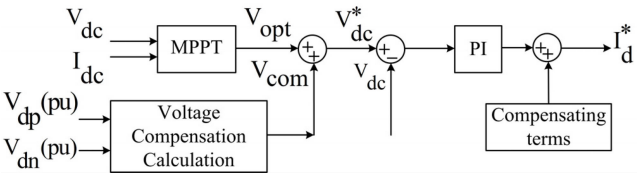

FIGURE 13. Control structure of the voltage compensation method.

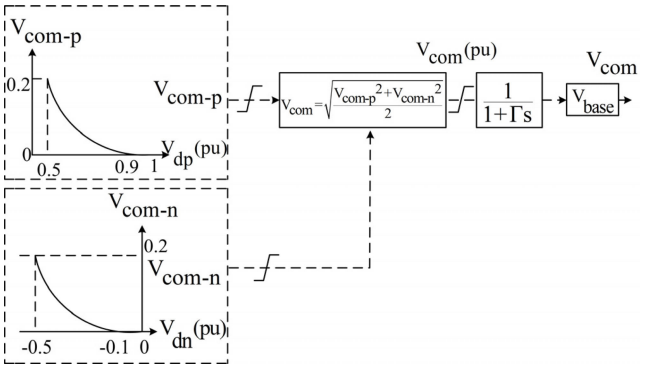

FIGURE 14. Voltage compensation calculation unit.

A voltage compensation calculation (VCC) unit is developed to curtail down the active power during voltage sag. A new dc-link reference (V_d^*) is obtained by adding a compensating value (V_{com}) to the optimum value (V_{opt}).

By taking the tolerance of 10%, the compensating voltage for the positive sequence is obtained as in (138)

$$V_{com-p} = -\Delta V_{dp}(V_{dp} - 0.9) \tag{138}$$

Similarly, the compensating voltage for negative sequence is obtained as in (139)

$$V_{com-n} = -\Delta V_{dn}(-V_{dn} - 0.1) \tag{139}$$

Here, V_{dp} and V_{dn} are the positive and negative sequence voltage of d component after fault, respectively. By utilizing (138) and (139) it is ensured that, the V_{dc}^* is always less than V_{oc}. where, V_{oc} is the open-circuit voltage of the PV array. The control and calculation unit of the voltage compensation method is shown in Figure 13 and 14, respectively.

B. KRUSH-KUHN-TUCKER BASED CONTROL (KKTBC)

Another optimization strategy in the d-q frame of reference to generate current references by employing Karush-Kuhn-Tucker (KKT) is proposed by [150]. This strategy is designed by considering the X/R ratio of the system which helps in differentiating between the weak and stiff grid. It also provides voltage support by enhancing the positive sequence component and minimizes the negative sequence component. To prevent the activation of overcurrent protection in the inverter, the necessary condition is given in (140).

$$I_{max} = \sqrt{I^{+2} + I^{-2}} = \max(I_{a(peak)}, I_{b(peak)}, I_{c(peak)}) \tag{140}$$

Although the condition in (140) is necessary, it does not guarantee the prevention of overcurrent protection. Hence, an inequality constraint of (141) is also considered as opposed

TABLE 6. Comparison between DC-link voltage control strategies under low-voltage-ride-through condition.

Reference, Strategy	Experimental results	Controller	dc-link voltage	Advantages	Disadvantages	THD	Efficiency	Accuracy	Power Factor	Network Losses	Dynamic Response
[127], ILPDS	No	PI	Fixed	• Injected currents are balanced and free from harmonics under faulty grid conditions • Both active and reactive powers are injected under unbalanced faults	• Oscillations in dc-link voltage due to asymmetrical voltage sags. • Dynamic response of the system is unknown	Low	High	Low	Low	Low	Poor
[135], DCVCIL	No	PI	Variable	• Improved system reliability • Enhanced power injection capability	• Large overshoot in reactive power under external disturbances	Low	High	High	High	Low	Poor
[136], FLCSMC	Yes	FLC	Fixed	• Robust under external disturbances • Does not require adjustment in the control gains like conventional PI controller	• Complex control structure	High	High	High	Low	High	Excellent
[137], NMMCPCC	No	PI	Fixed	• Simple structure as PWM module and PI controller is not required • Elimination of harmonics in dc-link voltage • Balanced currents are injected to the grid	• Sustained oscillations in both real and reactive power	Low	High	High	High	Low	Poor
[142], IDCR	Yes	PI	Fixed	• Reduced cost as dc-link current sensor is absent • No chattering in the dc-link voltage • Good performance under external disturbances	• Reactive power injection is not considered under unbalanced grid faults	Low	Low	High	-	High	Poor
[143], PSODCVC	No	PI-PSO	Fixed	• Improved dynamic performance • High efficiency	• High cost • Increased computation complexity	Low	Low	High	High	Low	Excellent
[144], WOADCVC	No	PI-MHT	Fixed			Low	High	High	High	Low	Excellent
[145], VDRBC	Yes	PI	Variable	• Full Attenuation of ripples in the dc-link voltage • Improve power controllability due to high modulation index	• In absence of capacitor optimization, the overshoot in current during voltage recovery is noticed	Low	High	High	High	Low	Poor
[146], IDFSOGI	Yes	PI	Variable	• Reduction in switching and ohmic losses • Reduced high frequency ripples in grid current • Increased power output	• Use of DFSOGI control algorithm makes the system more complex.	Low	High	High	High	Low	Excellent
[147], CPIDCVC	Yes	PI	Variable	• Low switching losses • Improved dynamic performance • Reduced THD in injected currents	• Reactive power injection is not considered under fault conditions • Sustained oscillations in dc-link voltage	Low	High	High	High	Low	Excellent
[148], IDCVC	Yes	PI	Variable	• Improved stability of the dc-link voltage control loop • Highly robust	• Non-linearity in the dc-link voltage is not considered	Low	High	High	High	Low	Excellent

to the strategy proposed in [54].

$$I_{max} \leq I_{oc} \tag{141}$$

where, I_{oc} is the overcurrent protection threshold that the inverter switches can sustain.

The optimal solutions by employing KKT are obtained as in (142) – (145).

$$\left(i_d^+\right)^* = I_{max}\frac{R}{\sqrt{R^2+(\omega L)^2}} \tag{142}$$

$$\left(i_q^+\right)^* = I_{max}\frac{\omega L}{\sqrt{R^2+(\omega L)^2}} \tag{143}$$

$$\left(i_d^-\right)^* = -I_{max}\frac{R}{\sqrt{R^2+(\omega L)^2}} \tag{144}$$

$$\left(i_q^-\right)^* = -I_{max}\frac{\omega L}{\sqrt{R^2+(\omega L)^2}} \tag{145}$$

C. ACTIVE AND REACTIVE CURRENT INJECTION BASED CONTROL (AARCIBC)

The disadvantages of the traditional LVRT control scheme are:

1) It is less effective for low voltage distribution networks (LVDN) as the resistive component is prominent in this type of network.
2) The existing resources are not fully utilized. The dc-link capacitor can be utilized to absorb or release a certain amount of energy in transient voltage event, which has not been pondered in previous works.

Considering the drawbacks of conventional strategies, an improved LVRT strategy for LVDN is proposed in [151]. In this, a mathematical analysis is carried out to prove that the active current injection (ACI) in LVDN with a high R/X ratio, is as effective as reactive current injection (RCI) in high X/R ratio networks to provide voltage support. Under normal operating conditions, RCI is employed to support the voltage at PCC. However, under severe grid fault, the ACI supports the PCC voltage in LVDN.

The optimization problem is formulated as in (146) – (150).

$$v = \left[I_{pv}^{ref}\, I_d^{ref}\, I_q^{ref}\, U_{dc}^{ref}\right]^T \tag{146}$$

Obj :

$$\arg\max\ I_d + E_{pv} \tag{147}$$

$$\text{Subject to } P_{pv}^{ref} \leq P_{pv}^{mpp} \tag{148}$$

$$I_q^{ref} = \min\left(2.\frac{\left|U_g - U_{rated}\right|}{U_{rated}}.I_{rated}, I_{rated}\right) \tag{149}$$

$$I_d^{ref} \leq \sqrt{1.1^2.I_{rated}^2 - I_q^{ref\,2}} \tag{150}$$

$$U_{dc}^{min} \leq U_{dc}^{ref} \leq U_{dc}^{max} \tag{151}$$

where, $\boldsymbol{v}$ is the vector of decision variables, which includes PV output current reference, current references of d and q component and reference dc-link voltage.

The main aim is to maximize the ACI during faults and PV energy harvesting. The environmental constraint in (145) ensures that PV reference power should not exceed the PV power at MPP under fault conditions. Using (149), I_q^{ref} is determined under LVRT condition, where U_g is the RMS phase voltage at PCC. To maximize the ACI, the maximum allowable output current of GCPV inverter is set to be 1.1 pu during unbalanced grid conditions. The maximum injected active power of the GCPV inverter is obtained as in (152).

$$P_g^{max} = \sqrt{1.1^2 - \left(2 - \frac{2U_g}{U_{rated}}\right)^2}.\frac{U_g}{U_{rated}}.P_o \tag{152}$$

where, P_o and U_{rated} are the rated output power and RMS phase voltage of GCPV inverter, respectively. Based on the different PCC voltage and environmental conditions, three modes of operations are proposed. In mode 1, when $U_g \geq 0.9$ pu, the PV generator works under normal operating conditions with MPPT execution.

In mode 2, when $U_g \leq 0.9$ pu, and $P_g^{max} \leq P_{pv}^{mpp}$, the PV inverter is operating under LVRT. It fulfills RCI requirements as per grid code and the remaining power capacity of the GCPV inverter is utilized through ACI. During this mode, the dc-link capacitor also stores some extra PV energy.

In mode 3, when $U_g \leq 0.9$ pu, and $P_g^{max} \geq P_{pv}^{mpp}$, LVRT control is activated and MPPT is maintained. Moreover, the dc-link voltage is released to fulfill the ACI requirements. In this mode to avoid over-modulation, in a three-phase system, the dc-link voltage is maintained as in (153).

$$U_{dc}^{ref} \geq U_{dc}^{min} = 2\sqrt{2}U_g \tag{153}$$

D. REACTIVE POWER SUPPORT WITH APC (RPSWAPC)

A strategy for a LV network with low X/R ratio is presented in [152]. The scheme presents novel reactive power support that works well for under and over voltage conditions by considering the grid impedance. The controller shifts to APC mode if the reactive power support is not sufficient to ensure the PCC voltage does not go beyond the over voltage limits. Injection of active power is given more priority than reactive power for better voltage support. To provide better voltage support, active power is reduced during over voltage conditions. Hence, the scheme also works well under high-voltage-ride-through (HVRT). Unlike conventional peak current limiter, this scheme directly calculates the peak values in injected current and minimizes the active and reactive power references. While minimizing the powers, reactive power is given more priority, however, under severe voltage sag, both power references are minimized.

Furthermore, under unbalanced grid conditions, it employs both sequence components for better voltage support. The strategy provides a smooth ride-through operation even for sudden grid faults, without any current overshoots.

The PCC voltage amplitude is given in (154) by assuming a small power angle.

$$V_{PCC} \cong V_g + \frac{(P_{PV} - P_L)\,R_g}{V_{PCC}} + \frac{(Q_{PV} - Q_L)\,X_g}{V_{PCC}} \tag{154}$$

To remove the active oscillations and reducing the ripples of dc-link voltage, the reference currents are formulated in

the d-q reference frame as in (155) – (158).

$$i_d^{ref^+} = \frac{2}{3}\left(\frac{v_d^+ P_{ref}}{V^{+2} - V^{-2}} + \frac{v_q^+ Q_{ref}}{V^{+2} + V^{-2}}\right) \quad (155)$$

$$i_q^{ref^+} = \frac{2}{3}\left(\frac{v_q^+ P_{ref}}{V^{+2} - V^{-2}} - \frac{v_d^+ Q_{ref}}{V^{+2} + V^{-2}}\right) \quad (156)$$

$$i_d^{ref^-} = \frac{2}{3}\left(-\frac{v_d^- P_{ref}}{V^{+2} - V^{-2}} + \frac{v_q^- Q_{ref}}{V^{+2} + V^{-2}}\right) \quad (157)$$

$$i_q^{ref^-} = \frac{2}{3}\left(-\frac{v_q^- P_{ref}}{V^{+2} - V^{-2}} - \frac{v_d^- Q_{ref}}{V^{+2} + V^{-2}}\right) \quad (158)$$

E. ACTIVE POWER BACKFLOW CONTROL STRATEGY (APBCS)

In [153], a control strategy is proposed that reduces the active power backflow in cascaded PV solid-state transformers (SST). As previously discussed, in the case of unbalanced voltage sags, there are three, positive, negative and zero sequence components. The sum of active powers generated by negative sequence voltage component on three-phase inverters is obtained as in (159).

$$P_{AN} + P_{BN} + P_{CN} = 0 \quad (159)$$

It is to be pointed out that the negative sequence component does not generate any additional active power but redistributes the active power in all three phases. According to (159) the active power generated by negative sequence voltage must be less than zero in a certain phase during LVRT. It is assumed that for phase A, P_{AN} is less than zero. Hence the total active power transmitted by phase A ($P_A = P_{AP} + P_{AN}$), will be less than zero. This indicates that Phase A will absorb the active power from the grid and is known as active power backflow.

In case of conventional PV inverters, active power generated by negative sequence voltage can return to the common dc bus and have negligible effect on the system. This means that the three level LLC inverter transmits power only in one direction. Hence, the power cannot be returned to the common dc bus and flows through the dc buses of H Bridge which creates overvoltage in phase A and causes shut down of PV SST due to overvoltage protection.

To overcome this power backflow issue in PV SST, two methods have been proposed in [153].

In the first method, the injected current does not contain zero sequence component and only large positive sequence active current is injected. Hence, the active power generated in X phase is greater than the absolute value of that phase which is generated by negative sequence voltage as in (160).

$$P_{XP} \geq |P_{XN}|; \quad P_{X0} = 0 \quad (160)$$

where, X denotes the phases A, B, C and $P_X = P_{XP} + P_{XN} \geq 0$.

The active power generated by positive sequence voltage is given as in (161).

$$P_{XP} = 0.5\, V_P I_g \cos\theta = 0.5\, V_P I_{dp} \leq P_T/3 \quad (161)$$

where, V_P is the amplitude of positive sequence grid voltages, I_g is the amplitude of grid currents, θ is the power factor angle of the PV inverter, I_{dp} is the active current due to positive sequence and P_T is the total power of the PV array. It is evident from (161) if I_{dp} increases, P_{XP} will also increase.

In the second method for a star-connected system, zero-sequence voltage is injected which does not provide excess current and active power and helps in distributing the active powers among the phases. Hence, zero-sequence voltage compensation balances out power redistribution of negative-sequence voltages which eliminates the active power backflow issue as in (162).

$$\begin{cases} P_{X0} = -P_{XN} \\ P_X = P_{XP} + P_{XN} + P_{X0};\ P_{XP} \geq 0 \end{cases} \quad (162)$$

This method also ensures that the active power flowing in each phase remains the same.

F. RECURRENT WAVELET FUZZY LOGIC NEURAL NETWORK BASED CONTROL (RWFLNNBC)

An improved LVRT technique designed for a weak grid is proposed in [154]. To control the active and reactive powers, recurrent wavelet fuzzy logic neural network (RWFNN) is employed, instead of conventional PI controllers. A three-level neutral-point clamped (NPC) inverter is employed where active and reactive power references are set according to the grid code.

The active and reactive power references are obtained as in (163) and (164), respectively.

$$P^* = |S|\sqrt{1 - I_r^*} \quad (163)$$

$$Q^* = |S|\, I_r^* \quad (164)$$

where, I_r^* is the reactive current reference, determined from the grid code. S is the maximum apparent power. The short circuit ratio (SCR) is defined as in (165).

$$SCR = \frac{S_{AC}}{S_N} \quad (165)$$

where, S_{AC} short circuit capacity of the AC system and S_N is the rated power of PV. The strategy considers that the value of SCR in weak grids is less than 3. Since low SCR values highly affect the grid voltage stability and power quality under grid faults, PI controllers are replaced by RWFNN controllers to improve the transient stability. The PI controllers are simple but not robust in terms of tackling the system uncertainties like modeling errors, parametric variations and other external disturbances. On the other hand, the RWFNN achieves superior dynamic modeling behavior, online learning and strong adaptive capability. The online learning algorithm is based on the backpropagation learning rule. The convergence of the tracking errors is determined by using the Lyapunov function. The RWFNN controller ensures smooth tracking responses and helps in reducing oscillations in active and reactive power.

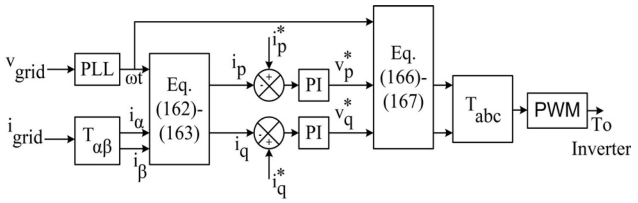

FIGURE 15. Block diagram of IPT control strategy.

G. INSTANTANEOUS POWER THEORY BASED CONTROL STRATEGY (IPTBCS)

In [155], a LVRT technique for reactive power injection is proposed based on instantaneous power theory (IPT). The strategy helps in improving the dynamic response from fault inception to fault clearance. The method also helps in reducing the size of the filter which helps in reducing the overall cost. Two types of controllers have been investigated, PI-IPT and fuzzy logic control (FLC)-IPT and it is found that the FLC-IPT has the better dynamic performance as compared to the PI-IPT. The PI-IPT and FLC-IPT controllers have a superior dynamic response than RWFNN, proposed in [146]. The block diagram of the IPT control strategy is shown in Figure 15.

According to IPT, the active and reactive currents are given as in (166) and (167), respectively.

$$i_p = i_\alpha \sin\omega t - i_\beta \cos\omega t \tag{166}$$

$$i_q = -i_\alpha \cos\omega t - i_\beta \sin\omega t \tag{167}$$

Furthermore, the active and reactive current references are obtained as in (168) and (169), respectively.

$$i_q^* = i_n \times i_q \tag{168}$$

$$i_p^* = i_n \times \sqrt{1 - i_q^2} \tag{169}$$

The error signals computed using the reference and actual values of active and reactive currents are passed through a PI controller to obtain active and reactive voltage references (v_p^*, v_q^*), respectively. Using this, the voltage references in $\alpha\beta$ reference are obtained as in (170) and (171), respectively.

$$v_\alpha = v_p^* \sin\omega t - v_q^* \cos\omega t \tag{170}$$

$$v_\beta = -v_p^* \cos\omega t - v_q^* \sin\omega t \tag{171}$$

Another problem faced during LVRT under unbalanced grid conditions is the voltage fluctuations at neutral point (NP) in a transformer-less three-level GCPV inverter. To minimize these fluctuations, a large, middle and zero vector modulation (LMZVM) strategy is utilized [156].

The removal of the transformer causes a ground current between the PV panel and the ground, which injects through the parasitic capacitance.

Moreover, it results in electromagnetic interference and distortion in grid current. By utilizing the LMZVM technique, a low common-mode voltage (neutral point (NP) voltage) is produced which in turn reduces the ground current. DC-DC Converters are also utilized to balance NP voltage, which increases the overall cost and size of the systems [157]. Using a large dc-link capacitance can be a solution to suppress the NP voltage, however, selecting dc-link capacitance for pure reactive power requires a very high value of capacitance [158]. Another strategy is proposed in [156] which balances the NP voltage by employing four weighing factors to determine the peak-to-peak values of NP voltage.

VI. FUTURE ASPECTS OF CONTROL STRATEGIES UNDER LVRT CONDITION

From the detailed literature survey presented in this study, related to the various challenges associated during LVRT, the following points should be considered while designing the control strategies:

1. There is scope to design a simple low-cost structure to improve the synchronization capability under unbalanced faults.
2. There is further scope in improving the performance of voltage support strategies underlying parameters variation such as X/R ratio.
3. Most researchers have designed control strategies for a single PV system. Much work can be done by considering multiple PV inverters and develop a holistic control strategy that can assist in voltage unbalance from a systemic standpoint
4. There is scope in developing voltage support control strategies that fulfill multiple objectives to mitigate power quality issues, like oscillations in active and reactive power, distortion and high peaks in the inverter currents.
5. The voltage support control strategies devised have mitigated the unbalance factor under constant power generation. Researchers need to consider variable power generation scenarios to practically visualize the performance of these control strategies.
6. More work can be done on designing a flexible current limitation strategy to fulfill the requirements of different available grid codes.
7. The current limitation strategies proposed by most researchers have considered the injection of active power under low generation scenarios. Further improvements can be achieved by considering the maximum injection of both active and reactive power with enhanced power quality.
8. Most researchers have devised dc-link control strategies under constant power generation. Further work can be done on designing dc-link strategies with improved dynamic response under variable power generation.
9. Most strategies have considered the injection of the negative sequence component. More work can be done by considering the zero-sequence component to provide better voltage support.
10. Most researchers have considered a constant dc-link voltage. There is further scope in designing a dc-link

control strategy by considering multiple generating sources to analyze a complete system.

11. Further work can be done by providing low-cost solutions to achieve constant or variable dc-link voltage while ensuring low switching losses in the system.
12. More work can be done on developing algorithms to provide active power curtailment by considering variation in irradiance under variable dc-link voltage.
13. Further research can be carried out in reducing the ripples in dc-link voltage to achieve better power balance by using advanced dc-dc converter topologies.

In a nutshell, future work should emphasize the design of control strategies from a systemic standpoint. The control strategies should be able to fulfill multiple objectives considering power quality issues under variable power generation. Finally, researchers should also focus on the stability aspects to completely analyze the performance of the system under internal and external disturbances.

VII. CONCLUSION

Several challenges are present during LVRT operation in GCPV inverters. Various strategies are reported in the literature to overcome these challenges. This paper mainly categorizes these strategies and discusses the performance of each strategy. The categorization is based on voltage support, current limitation and dc-link voltage control.

The voltage support control strategies present in the literature are designed based on the type of grid. Some VSS help in providing voltage equalization but results in high THD and poor dynamic response. Other VSSs inject both active and reactive power for enhanced voltage support but have challenges in tuning the controller. Another strategy simultaneously provides voltage support and current limitation but results in sustained oscillations in reactive power. Few other strategies have been discussed that have low THD and improved power factor but results in network losses and suffer from poor dynamic response.

The current limitation strategies discussed help in limiting the overcurrent in the faulty phase to prevent activation of inverter overcurrent protection. A CLS is designed by curtailing the PV power but has large oscillations in the reactive power. Another strategy exploits the maximum rating of the inverter and provides zero oscillations in active power and injects unbalanced currents. Yet another strategy helps in current limitation but provides no regulation on the minimum set point in the reduction of inverter overcurrent and does not exploit the full capability of the inverter. There are other strategies that improve the voltage support at PCC as well as provide current limitation with poor accuracy and result in oscillations in active and reactive power.

The dc-link voltage control strategy is further categorized into constant and adaptive. The constant dc-link strategies help in injecting balanced current within the system but result in oscillations in the dc-link voltage under asymmetrical faults. The adaptive dc-link strategies help in reducing the ripples in the dc-link voltage with low switching and ohmic losses in the inductor but result in large overshoot under external disturbances.

The control strategies present in the literature have only analyzed the performance under constant power generation during LVRT condition. The power quality issues, like oscillations in active, reactive powers and dc-link voltage along with THD in currents, efficiency, accuracy and stability aspects should be simultaneously tackled. Some strategies use the filtering capability of the PLLs to determine the sag under unbalanced grid voltage conditions. However, this additional filtering results in an increased computational burden on the system. Some additional strategies have also been discussed that help in overcoming challenges during LVRT such as active power backflow and voltage fluctuations at NP in transformer-less PV inverter.

Further future avenues for research have been pointed out that can be used to tackle power quality issues under variable power generation conditions. The categorization and comparison of these control strategies would prove to be beneficial for engineers, system operators, and researchers working in this area.

REFERENCES

[1] S. Krithiga and N. G. A. Gounden, "Power electronic configuration for the operation of PV system in combined grid-connected and stand-alone modes," *IET Power Electron.*, vol. 7, no. 3, pp. 640–647, Mar. 2014.

[2] K. Mahmoud and M. Lehtonen, "Comprehensive analytical expressions for assessing and maximizing technical benefits of photovoltaics to distribution systems," *IEEE Trans. Smart Grid*, early access, Jul. 15, 2021, doi: 10.1109/TSG.2021.3097508.

[3] E. Serban, M. Ordonez, and C. Pondiche, "Voltage and frequency grid support strategies beyond standards," *IEEE Trans. Power Electron.*, vol. 32, no. 1, pp. 298–309, Jan. 2017.

[4] C.-Y. Tang, Y.-T. Chen, and Y.-M. Chen, "PV power system with multimode operation and low-voltage ride-through capability," *IEEE Trans. Ind. Electron.*, vol. 62, no. 12, pp. 7524–7533, Dec. 2015.

[5] I. I. Perpinias, N. P. Papanikolaou, and E. C. Tatakis, "Fault ride through concept in low voltage distributed photovoltaic generators for various dispersion and penetration scenarios," *Sustain. Energy Technol. Assessments*, vol. 12, pp. 15–25, Dec. 2015.

[6] P. Mishra, A. K. Pradhan, and P. Bajpai, "Voltage control of PV inverter connected to unbalanced distribution system," *IET Renew. Power Gener.*, vol. 13, no. 9, pp. 1587–1594, Apr. 2019.

[7] V. L. Srinivas, B. Singh, and S. Mishra, "Fault ride-through strategy for two-stage grid-connected photovoltaic system enabling load compensation capabilities," *IEEE Trans. Ind. Electron.*, vol. 66, no. 11, pp. 8913–8924, Nov. 2019.

[8] M. El-Shimy, A. Sharaf, H. Khairy, and G. Hashem, "Reduced-order modelling of solar-PV generators for small-signal stability assessment of power systems and estimation of maximum penetration levels," *IET Gener. Transm. Distrib.*, vol. 12, no. 8, pp. 1838–1847, Apr. 2018.

[9] V. Jately, B. Azzopardi, J. Joshi, B. Venkateswaran, A. Sharma, and S. Arorab, "Experimental analysis of hill-climbing MPPT algorithms under low irradiance levels," *Renew. Sust. Energ. Rev.*, vol. 150, Oct. 2021, Art. no. 111467.

[10] V. Jately and S. Arora, "An efficient hill-climbing technique for peak power tracking of photovoltaic systems," in *Proc. IEEE 7th Power India Int. Conf. (PIICON)*, Bikaner, India, Nov. 2016, pp. 1–5.

[11] V. Jately and S. Arora, "Performance investigation of hill-climbing MPPT techniques for PV systems under rapidly changing environment," in *Advances in Intelligent Systems and Computing*. Singapore: Springer, 2018, pp. 1145–1157.

[12] V. Jately and S. Arora, "Development of a dual-tracking technique for extracting maximum power from PV systems under rapidly changing environmental conditions," *Energy*, vol. 133, pp. 557–571, Aug. 2017.

[13] N. Jaalam, N. A. Rahim, A. H. A. Bakar, and B. M. Eid, "Strategy to enhance the low-voltage ride-through in photovoltaic system during multi-mode transition," *Sol. Energy*, vol. 153, pp. 744–754, Sep. 2017.

[14] A. Q. Al-Shetwi, M. Z. Sujod, and F. Blaabjerg, "Low voltage ride-through capability control for single-stage inverter-based grid-connected photovoltaic power plant," *Solar Energy*, vol. 159, pp. 665–681, Jan. 2018.

[15] *Grid Code High and Extra High Voltage*, E.ON Netz GmbH, Bayreuth, Germany, Aug. 2003.

[16] A. Q. Al-Shetwi and M. Z. Sujod, "Grid-connected photovoltaic power plants: A review of the recent integration requirements in modern grid codes," *Int. J. Energy Res.*, vol. 42, no. 5, pp. 1849–1865, Apr. 2018.

[17] Y. Yang, P. Enjeti, F. Blaabjerg, and H. Wang, "Suggested grid code modifications to ensure wide-scale adoption of photovoltaic energy in distributed power generation systems," in *Proc. IEEE Ind. Appl. Soc. Annu. Meeting*, Lake Buena Vista, FL, USA, Oct. 2013, pp. 1–8.

[18] Y. Yang, P. Enjeti, F. Blaabjerg, and H. Wang, "Wide-scale adoption of photovoltaic energy: Grid code modifications are explored in the distribution grid," *IEEE Ind. Appl. Mag.*, vol. 21, no. 5, pp. 21–31, Sep. 2015.

[19] M. Y. Worku and M. A. Abido, "Grid-connected PV array with supercapacitor energy storage system for fault ride through," in *Proc. IEEE Int. Conf. Ind. Technol. (ICIT)*, Seville, Spain, Mar. 2015, pp. 2901–2906.

[20] L. Chen, H. Chen, Y. Li, G. Li, J. Yang, X. Liu, Y. Xu, L. Ren, and Y. Tang, "SMES-battery energy storage system for the stabilization of a photovoltaic-based microgrid," *IEEE Trans. Appl. Supercond.*, vol. 28, no. 4, Jun. 2018, Art. no. 5700407.

[21] A. Q. Al-Shetwi, M. Z. Sujod, F. Blaabjerg, and Y. Yang, "Fault ride-through control of grid-connected photovoltaic power plants: A review," *Sol. Energy*, vol. 180, pp. 340–350, Mar. 2019.

[22] S. Xiangdong, R. Biying, Z. Qi, and A. Shaoliang, *Solar Grid-Connected Photovoltaic Power Generation Technology* (Low-Voltage Ride-Through Control Methods). New Delhi, India: Roy. Collins, 2020.

[23] G. Lammert, *Modelling, Control and Stability Analysis of Photovoltaic Systems in Power System Dynamic Studies*. Kassel, Germany: Kassel Univ. Press, Jun. 2019.

[24] F.-J. Lin, K.-C. Lu, T.-H. Ke, B.-H. Yang, and Y.-R. Chang, "Reactive power control of three-phase grid-connected PV system during grid faults using Takagi–Sugeno–Kang probabilistic fuzzy neural network control," *IEEE Trans. Ind. Electron.*, vol. 62, no. 9, pp. 5516–5528, Sep. 2015.

[25] N. H. Saad, A. A. El-Sattar, and A. E.-A. M. Mansour, "Improved particle swarm optimization for photovoltaic system connected to the grid with low voltage ride through capability," *Renew. Energy*, vol. 85, pp. 181–194, Jan. 2016.

[26] A. Mojallal and S. Lotfifard, "Enhancement of grid connected PV arrays fault ride through and post fault recovery performance," *IEEE Trans. Smart Grid*, vol. 10, no. 1, pp. 546–555, Jan. 2019.

[27] M. Easley, S. Jain, M. Shadmand, and H. Abu-Rub, "Autonomous model predictive controlled smart inverter with proactive grid fault ride-through capability," *IEEE Trans. Energy Convers.*, vol. 35, no. 4, pp. 1825–1836, Dec. 2020.

[28] Y. Wang and B. Ren, "Fault ride-through enhancement for grid-tied PV systems with robust control," *IEEE Trans. Ind. Electron.*, vol. 65, no. 3, pp. 2302–2312, Mar. 2018.

[29] Y. Zhang, J. Wang, H. Li, T. Q. Zheng, J.-S. Lai, J. Li, J. Wang, and Q. Chen, "Dynamic performance improving sliding-mode control-based feedback linearization for PV system under LVRT condition," *IEEE Trans. Power Electron.*, vol. 35, no. 11, pp. 11745–11757, Nov. 2020.

[30] I. R. S. Priyamvada and S. Das, "Online assessment of transient stability of grid connected PV generator with DC link voltage and reactive power control," *IEEE Access*, vol. 8, pp. 220606–220619, 2020.

[31] H. Tian, F. Gao, C. Ma, G. He, and G. Li, "A review of low voltage ride-through techniques for photovoltaic generation systems," in *Proc. IEEE Energy Convers. Congr. Expo. (ECCE)*, Pittsburgh, PA, USA, Sep. 2014, pp. 1566–1572.

[32] R. Shah, N. Mithulananthan, R. C. Bansal, and V. K. Ramachandaramurthy, "A review of key power system stability challenges for large-scale PV integration," *Renew. Sustain. Energy Rev.*, vol. 41, pp. 1423–1436, Jan. 2015.

[33] J. Jia, G. Yang, and A. H. Nielsen, "A review on grid-connected converter control for short-circuit power provision under grid unbalanced faults," *IEEE Trans. Power Del.*, vol. 33, no. 2, pp. 649–661, Apr. 2018.

[34] M. Tarafdar Hagh and T. Khalili, "A review of fault ride through of PV and wind renewable energies in grid codes," *Int. J. Energy Res.*, vol. 43, no. 4, pp. 1342–1356, Mar. 2019.

[35] M. Z. I. Sarkar, L. G. Meegahapola, and M. Datta, "Reactive power management in renewable rich power grids: A review of grid-codes, renewable generators, support devices, control strategies and optimization algorithms," *IEEE Access*, vol. 6, pp. 41458–41489, 2018.

[36] X. Zhao, L. Chang, R. Shao, and K. Spence, "Power system support functions provided by smart inverters—A review," *CPSS Trans. Power Electron. Appl.*, vol. 3, no. 1, pp. 25–35, Mar. 2018.

[37] B. R. Naidu, P. Bajpai, and C. Chakraborty, "Voltage fault ride-through operation of solar PV units: A review and way forward," in *Proc. 8th Int. Conf. Power Syst. (ICPS)*, Jaipur, India, Dec. 2019, pp. 1–6.

[38] M. Sufyan, N. A. Rahim, B. Eid, and S. R. S. Raihan, "A comprehensive review of reactive power control strategies for three phase grid connected photovoltaic systems with low voltage ride through capability," *J. Renew. Sustain. Energy*, vol. 11, no. 4, Jul. 2019, Art. no. 042701.

[39] Z. Hassan, A. Amir, J. Selvaraj, and N. A. Rahim, "A review on current injection techniques for low-voltage ride-through and grid fault conditions in grid-connected photovoltaic system," *Sol. Energy*, vol. 207, pp. 851–873, Sep. 2020.

[40] M. Talha, A. Amir, S. R. S. Raihan, and N. Abd Rahim, "Grid-connected photovoltaic inverters with low-voltage ride through for a residential-scale system: A review," *Int. Trans. Electr. Energy Syst.*, vol. 4, pp. 1–28, Sep. 2020.

[41] A. Q. Al-Shetwi, M. A. Hannan, K. P. Jern, M. Mansur, and T. M. I. Mahlia, "Grid-connected renewable energy sources: Review of the recent integration requirements and control methods," *J. Cleaner Prod.*, vol. 253, Apr. 2020, Art. no. 119831.

[42] A. S. Vijay, S. Doolla, and M. C. Chandorkar, "Unbalance mitigation strategies in microgrids," *IET Power Electron.*, vol. 13, no. 9, pp. 1687–1710, Jul. 2020.

[43] L. S. Xavier, A. F. Cupertino, and H. A. Pereira, "Ancillary services provided by photovoltaic inverters: Single and three phase control strategies," *Comput. Electr. Eng.*, vol. 70, pp. 102–121, Aug. 2018.

[44] M. M. Shabestary, S. Mortazavian, and Y. I. Mohamed, "Overview of voltage support strategies in grid-connected VSCs under unbalanced grid faults considering LVRT and HVRT requirements," in *Proc. IEEE Int. Conf. Smart Energy Grid Eng. (SEGE)*, Oshawa, ON, Canada, Aug. 2018, pp. 145–149.

[45] P. Naresh and V. S. S. Kumar, "Analysis of low voltage ride through techniques for grid-connected photovoltaic systems," in *Proc. IEEE Int. Conf. Power Electron., Smart Grid Renew. Energy (PESGRE)*, Cochin, India, Jan. 2020, pp. 1–7.

[46] M. Parvez, M. F. M. Elias, N. A. Rahim, and N. Osman, "Current control techniques for three-phase grid interconnection of renewable power generation systems: A review," *Sol. Energy*, vol. 135, pp. 29–42, Oct. 2016.

[47] O. P. Mahela and A. G. Shaik, "Comprehensive overview of grid interfaced solar photovoltaic systems," *Renew. Sustain. Energy Rev.*, vol. 68, pp. 316–332, Feb. 2017.

[48] A. Rajendran, N. R. Nair, and P. Kanakasabapathy, "Inverter control strategies in solar PV systems with adaptive DC link technology—A review," in *Proc. Int. Conf. Control, Power, Commun. Comput. Technol. (ICCPCCT)*, Kannur, India, Mar. 2018, pp. 278–282.

[49] R. Panigrahi, S. K. Mishra, S. C. Srivastava, A. K. Srivastava, and N. N. Schulz, "Grid integration of small-scale photovoltaic systems in secondary distribution network—A review," *IEEE Trans. Ind. Appl.*, vol. 56, no. 3, pp. 3178–3195, May 2020.

[50] Y. Yang, H. Wang, and F. Blaabjerg, "Reactive power injection strategies for single-phase photovoltaic systems considering grid requirements," *IEEE Trans. Ind. Appl.*, vol. 50, no. 6, pp. 4065–4076, Nov./Dec. 2014.

[51] K. H. Oon, C. Tan, A. H. A. Bakar, H. S. Che, H. Mokhlis, and H. A. Illias, "Establishment of fault current characteristics for solar photovoltaic generator considering low voltage ride through and reactive current injection requirement," *Renew. Sustain. Energy Rev.*, vol. 92, pp. 478–488, Sep. 2018.

[52] H. Wen and M. Fazeli, "A low-voltage ride-through strategy using mixed potential function for three-phase grid-connected PV systems," *Electr. Power Syst. Res.*, vol. 173, pp. 271–280, Aug. 2019.

[53] G. Lammert, T. Hess, M. Schmidt, P. Schegner, and M. Braun, "Dynamic grid support in low voltage grids—Fault ride-through and reactive power/voltage support during grid disturbances," in *Proc. Power Syst. Comput. Conf.*, Wroclaw, Poland, Aug. 2014, pp. 1–7.

[54] R. Teodorescu, M. Liserre, and P. Rodriguez, *Grid Converters for Photovoltaic and Wind Power Systems* (Control of Grid Converters under Grid Faults). Hoboken, NJ, USA: Wiley, 2011.
[55] P. Rodriguez, J. Pou, J. Bergas, J. I. Candela, R. P. Burgos, and D. Boroyevich, "Decoupled double synchronous reference frame PLL for power converters control," *IEEE Trans. Power Electron.*, vol. 22, no. 2, pp. 584–592, Mar. 2007.
[56] M. Karimi-Ghartemani and M. R. Iravani, "A method for synchronization of power electronic converters in polluted and variable-frequency environments," *IEEE Trans. Power Syst.*, vol. 19, no. 3, pp. 1263–1270, Aug. 2004.
[57] S. Golestan, J. M. Guerrero, A. Vidal, A. G. Yepes, and J. Doval-Gandoy, "PLL with MAF-based prefiltering stage: Small-signal modeling and performance enhancement," *IEEE Trans. Power Electron.*, vol. 31, no. 6, pp. 4013–4019, Jun. 2016.
[58] X. Guo, W. Wu, and Z. Chen, "Multiple-complex coefficient-filter-based phase-locked loop and synchronization technique for three-phase grid-interfaced converters in distributed utility networks," *IEEE Trans. Ind. Electron.*, vol. 58, no. 4, pp. 1194–1204, Apr. 2011.
[59] P. Rodriguez, R. Teodorescu, I. Candela, A. V. Timbus, M. Liserre, and F. Blaabjerg, "New positive-sequence voltage detector for grid synchronization of power converters under faulty grid conditions," in *Proc. 37th IEEE Power Electron. Specialists Conf.*, Jeju, South Korea, Jun. 2006, pp. 1–7.
[60] S. Golestan, M. Monfared, and F. D. Freijedo, "Design-oriented study of advanced synchronous reference frame phase-locked loops," *IEEE Trans. Power Electron.*, vol. 28, no. 2, pp. 765–778, Feb. 2013.
[61] A. Nouralinejad, A. Bagheri, M. Mardaneh, and M. Malekpour, "Improving the decoupled double SRF PLL for grid connected power converters," in *Proc. 5th Annu. Int. Power Electron., Drive Syst. Technol. Conf. (PEDSTC)*, Tehran, Iran, Feb. 2014, pp. 347–352.
[62] F. Liccardo, P. Marino, and G. Raimondo, "Robust and fast three-phase PLL tracking system," *IEEE Trans. Ind. Electron.*, vol. 58, no. 1, pp. 221–231, Jan. 2011.
[63] S. Golestan, J. M. Guerrero, and A. M. Abusorrah, "MAF-PLL with phase-lead compensator," *IEEE Trans. Ind. Electron.*, vol. 62, no. 6, pp. 3691–3695, Jun. 2015.
[64] M. Ramezani, S. Golestan, S. Li, and J. M. Guerrero, "A simple approach to enhance the performance of complex-coefficient filter-based PLL in grid-connected applications," *IEEE Trans. Ind. Electron.*, vol. 65, no. 6, pp. 5081–5085, Jun. 2018.
[65] G. Sun, Y. Li, W. Jin, S. Li, and Y. Gao, "A novel low voltage ride-through technique of three-phase grid-connected inverters based on a nonlinear phase-locked loop," *IEEE Access*, vol. 7, pp. 66609–66622, 2019.
[66] S. Golestan, J. M. Guerrero, and J. C. Vasquez, "Three-phase PLLs: A review of recent advances," *IEEE Trans. Power Electron.*, vol. 32, no. 3, pp. 1894–1907, Mar. 2017.
[67] A. Luna, J. Rocabert, J. I. Candela, J. R. Hermoso, and R. Teodorescu, "Grid voltage synchronization for distributed generation systems under grid fault conditions," *IEEE Trans. Ind. Appl.*, vol. 51, no. 4, pp. 3414–3425, Jul. 2015.
[68] F. Blaabjerg and D. M. Ionel, *Renewable Energy Devices and Systems with Simulations in MATLAB and Ansysr*. Oxfordshire, U.K.: Taylor & Francis, 2020.
[69] Z. Dai, H. Lin, H. Yin, and Y. Qiu, "A novel method for voltage support control under unbalanced grid faults and grid harmonic voltage disturbances," *IET Power Electron.*, vol. 8, no. 8, pp. 1377–1385, Aug. 2015.
[70] X. Guo, W. Liu, X. Zhang, X. Sun, Z. Lu, and J. M. Guerrero, "Flexible control strategy for grid-connected inverter under unbalanced grid faults without PLL," *IEEE Trans. Power Electron.*, vol. 30, no. 4, pp. 1773–1778, Apr. 2015.
[71] A. Sabir and S. Ibrir, "A robust control scheme for grid-connected photovoltaic converters with low-voltage ride-through ability without phase-locked loop," *ISA Trans.*, vol. 96, pp. 287–298, Jan. 2020.
[72] M. Mirhosseini, J. Pou, and V. G. Agelidis, "Grid-connected photovoltaic power plant without phase angle synchronization able to address fault-ride-through capability," *IEEE J. Emerg. Sel. Topics Power Electron.*, vol. 8, no. 4, pp. 3467–3476, Dec. 2020.
[73] Y. Han, Y. Feng, P. Yang, L. Xu, Y. Xu, and F. Blaabjerg, "Cause, classification of voltage sag, and voltage sag emulators and applications: A comprehensive overview," *IEEE Access*, vol. 8, pp. 1922–1934, 2020.
[74] *IEEE Standard for Interconnecting Distributed Resources with Electric Power Systems*, Standard 1547-2003, Jul. 2003.
[75] *IEEE Recommended Practice for Utility Interface of Photovoltaic (PV) Systems*, Standard 929-2000, 2000.
[76] P. Rodriguez, A. V. Timbus, R. Teodorescu, M. Liserre, and F. Blaabjerg, "Flexible active power control of distributed power generation systems during grid faults," *IEEE Trans. Ind. Electron.*, vol. 54, no. 5, pp. 2583–2592, Oct. 2007.
[77] Y. Yang, K. A. Kim, F. Blaabjerg, A. Sangwongwanich, *Advances in Grid Connected Photovoltaic Power conversion Systems*. Chicago, IL, USA: Woodhead, 2019.
[78] H. M. Hasanien, "An adaptive control strategy for low voltage ride through capability enhancement of grid-connected photovoltaic power plants," *IEEE Trans. Power Syst.*, vol. 31, no. 4, pp. 3230–3237, Jul. 2016.
[79] A. Yazdani and R. Iravani, "Voltage-sourced converters in power systems," in *Modeling, Control, and Applications*. Hoboken, NJ, USA: Wiley, 2010.
[80] B. Singh, A. Chandra, and K. Al-Haddad, *Power Quality: Problems and Mitigation Techniques*. Hoboken, NJ, USA: Wiley, 2015.
[81] M. P. Kazmierkowski, R. Krishnan, F. Blaabjerg, *Control in Power Electronics: Selected Problems*. Amsterdam, The Netherlands: Elsevier, 2002.
[82] P. Sochor, N. M. L. Tan, and H. Akagi, "Low-voltage-ride-through control of a modular multilevel single-delta bridge-cell (SDBC) inverter for utility-scale photovoltaic systems," *IEEE Trans. Ind. Appl.*, vol. 54, no. 5, pp. 4739–4751, Sep. 2018.
[83] J. Shi, L. Ji, Q. Hong, Y. Mi, Z. Cao, A. Khan, and C. Booth, "A new control method for three phase inverters under unsymmetrical voltage sag conditions," in *Proc. IEEE 8th Int. Conf. Adv. Power Syst. Autom. Protection (APAP)*, Xi'an, China, Oct. 2019, pp. 991–995.
[84] J. Qiang, T.-W. Tsai, L. Hagemann, Z. Yang, B. Mortimer, and R. W. De Doncker, "Control strategies for robust low-voltage ride-through operation of grid-tied PV inverters," in *Proc. 5th IEEE Workshop Electron. Grid (eGRID)*, Aachen, Germany, Apr. 2020, pp. 1–6.
[85] A. Camacho, M. Castilla, J. Miret, J. C. Vasquez, and E. Alarcon-Gallo, "Flexible voltage support control for three-phase distributed generation inverters under grid fault," *IEEE Trans. Ind. Electron.*, vol. 60, no. 4, pp. 1429–1441, Apr. 2013.
[86] A. Camacho, M. Castilla, J. Miret, J. Matas, E. Alarcon-Gallo, L. G. de Vicuna, and P. Marti, "Reactive power control for voltage support during type c voltage-sags," in *Proc. 38th Annu. Conf. Ind. Electron. Soc.*, Montreal, QC, Canada, Oct. 2012, pp. 3462–3467.
[87] J. Miret, A. Camacho, M. Castilla, L. G. de Vicuña, and J. Matas, "Control scheme with voltage support capability for distributed generation inverters under voltage sags," *IEEE Trans. Power Electron.*, vol. 28, no. 11, pp. 5252–5262, Nov. 2013.
[88] A. Camacho, M. Castilla, J. Miret, R. Guzman, and A. Borrell, "Reactive power control for distributed generation power plants to comply with voltage limits during grid faults," *IEEE Trans. Power Electron.*, vol. 29, no. 11, pp. 6224–6234, Nov. 2014.
[89] Y. Wang, P. Yang, and Z. Xu, "Flexible voltage support control with imbalance mitigation capability for inverter-based distributed generation power plants under grid faults," *J. Power Electron.*, vol. 16, no. 4, pp. 1551–1564, Jul. 2016.
[90] M. Mirhosseini, J. Pou, and V. G. Agelidis, "Individual phase current control with the capability to avoid overvoltage in grid-connected photovoltaic power plants under unbalanced voltage sags," *IEEE Trans. Power Electron.*, vol. 30, no. 10, pp. 5346–5351, Oct. 2015.
[91] *Rules and Transition Periods for Specific Requirements in Addition to the Technical Guideline*, Generating Plants Connected to Medium Voltage Network - Guidelines for Generating Plants, Library, G. B. Pant Univ. Agricult. Technol., Pantnagar, India, Jun. 2008.
[92] M. M. Shabestary and Y. A. I. Mohamed, "Advanced voltage support and active power flow control in grid-connected converters under unbalanced conditions," *IEEE Trans. Power Electron.*, vol. 33, no. 2, pp. 1855–1864, Feb. 2018.
[93] A. Camacho, M. Castilla, J. Miret, L. G. de Vicuna, and R. Guzman, "Positive and negative sequence control strategies to maximize the voltage support in resistive–inductive grids during grid faults," *IEEE Trans. Power Electron.*, vol. 33, no. 6, pp. 5362–5373, Jun. 2018.
[94] A. Camacho, M. Castilla, J. Miret, L. G. de Vicuna, and G. L. M. Andres, "Control strategy for distribution generation inverters to maximize the voltage support in the lowest phase during voltage sags," *IEEE Trans. Ind. Electron.*, vol. 65, no. 3, pp. 2346–2355, Mar. 2018.
[95] A. Camacho, M. Castilla, J. Miret, P. Marti, and M. Velasco, "Maximizing positive sequence voltage support in inductive-resistive grids for distributed generation inverters during voltage sags," in *Proc. 42nd Annu. Conf. Ind. Electron. Soc.*, Florence, Italy, Oct. 2016, pp. 2343–2348.

[96] J. Miret, A. Camacho, M. Castilla, J. L. García de Vicuña, and J. Hoz, "Reactive current injection protocol for low-power rating distributed generation sources under voltage sags," *IET Power Electron.*, vol. 8, no. 6, pp. 879–886, Jun. 2015.

[97] J. Miret, M. A. Garnica, M. Castilla, J. L. Garcia de Vicuña, and A. Camacho, "PI-based controller for low-power distributed inverters to maximise reactive current injection while avoiding over voltage during voltage sags," *IET Power Electron.*, vol. 12, no. 1, pp. 83–91, Jan. 2019.

[98] D. Çelik and M. E. Meral, "Voltage support control strategy of grid-connected inverter system under unbalanced grid faults to meet fault ride through requirements," *IET Gener., Transmiss. Distrib.*, vol. 14, no. 16, pp. 3198–3210, Aug. 2020.

[99] M. Garnica, L. G. de Vicuna, J. Miret, M. Castilla, and R. Guzman, "Optimal voltage-support control for distributed generation inverters in RL grid-faulty networks," *IEEE Trans. Ind. Electron.*, vol. 67, no. 10, pp. 8405–8415, Oct. 2020.

[100] N. Afrin, F. Yang, and J. Lu, "Voltage support strategy for PV inverter to enhance dynamic voltage stability of islanded microgrid," *Int. J. Electr. Power Energy Syst.*, vol. 121, pp. 1–10, Oct. 2020.

[101] H. Liu, J. Zhou, W. Wang, and D. Xu, "Droop control scheme of a three-phase inverter for grid voltage unbalance compensation," *J. Power Electron.*, vol. 18, no. 4, pp. 1245–1254, Jul. 2018.

[102] Y. Zhang, M. G. L. Roes, M. A. M. Hendrix, and J. L. Duarte, "Symmetric-component decoupled control of grid-connected inverters for voltage unbalance correction and harmonic compensation," *Int. J. Electr. Power Energy Syst.*, vol. 115, Feb. 2020, Art. no. 105490.

[103] H. D. Tafti and A. I. Maswood, "A review of active/reactive power control strategies for PV power plants under unbalanced grid faults," in *Proc. IEEE Innov. Smart Grid Technol.-Asia (ISGT ASIA)*, Bangkok, Thailand, Nov. 2015, pp. 1–6.

[104] S. R. Mohapatra and V. Agarwal, "An advanced voltage support scheme considering the impact of zero-sequence voltage under microgrid faults using model predictive control," *IEEE Trans. Ind. Electron.*, vol. 67, no. 10, pp. 8957–8968, Oct. 2020.

[105] M. M. Ghahderijani, A. Camacho, C. Moreira, M. Castilla, and L. G. de Vicuna, "Imbalance-voltage mitigation in an inverter-based distributed generation system using a minimum current-based control strategy," *IEEE Trans. Power Del.*, vol. 35, no. 3, pp. 1399–1409, Jun. 2020.

[106] M. Castilla, J. Miret, J. L. Sosa, J. Matas, and L. G. de Vicuña, "Grid-fault control scheme for three-phase photovoltaic inverters with adjustable power quality characteristics," *IEEE Trans. Power Electron.*, vol. 25, no. 12, pp. 2930–2940, Dec. 2010.

[107] J. Miret, M. Castilla, A. Camacho, L. G. de Vicuña, and J. Matas, "Control scheme for photovoltaic three-phase inverters to minimize peak currents during unbalanced grid-voltage sags," *IEEE Trans. Power Electron.*, vol. 27, no. 10, pp. 4262–4271, Oct. 2012.

[108] C. T. Lee, C. W. Hsu, and P. T. Cheng, "A low-voltage ride-through technique for grid-connected converters of distributed energy resources," *IEEE Trans. Ind. Appl.*, vol. 47, no. 4, pp. 1821–1832, Jul. 2011.

[109] K. Ma, M. Liserre, and F. Blaabjerg, "Power controllability of three-phase converter with unbalanced AC source," in *Proc. 28th Annu. Appl. Power Electron. Conf. Expo. (APEC)*, Long Beach, CA, USA, Mar. 2013, pp. 342–350.

[110] A. Camacho, M. Castilla, J. Miret, A. Borrell, and L. G. de Vicuna, "Active and reactive power strategies with peak current limitation for distributed generation inverters during unbalanced grid faults," *IEEE Trans. Ind. Electron.*, vol. 62, no. 3, pp. 1515–1525, Mar. 2015.

[111] A. Camacho, M. Castilla, J. Miret, J. Matas, R. Guzman, O. de Sousa-Perez, P. Marti, and L. G. de Vicuna, "Control strategies based on effective power factor for distributed generation power plants during unbalanced grid voltage," in *Proc. 39th Annu. Conf. Ind. Electron. Soc.*, Vienna, Austria, Nov. 2013, pp. 7134–7139.

[112] H.-C. Chen, C.-T. Lee, P.-T. Cheng, R. Teodorescu, and F. Blaabjerg, "A low-voltage ride-through technique for grid-connected converters with reduced power transistors stress," *IEEE Trans. Power Electron.*, vol. 31, no. 12, pp. 8562–8571, Dec. 2016.

[113] X. Guo, W. Liu, and Z. Lu, "Flexible power regulation and current-limited control of the grid-connected inverter under unbalanced grid voltage faults," *IEEE Trans. Ind. Electron.*, vol. 64, no. 9, pp. 7425–7432, Sep. 2017.

[114] X. Du, Y. Wu, S. Gu, H.-M. Tai, P. Sun, and Y. Ji, "Power oscillation analysis and control of three-phase grid-connected voltage source converters under unbalanced grid faults," *IET Power Electron.*, vol. 9, no. 11, pp. 2162–2173, 2016.

[115] E. Afshari, G. R. Moradi, R. Rahimi, B. Farhangi, Y. Yang, F. Blaabjerg, and S. Farhangi, "Control strategy for three-phase grid-connected PV inverters enabling current limitation under unbalanced faults," *IEEE Trans. Ind. Electron.*, vol. 64, no. 11, pp. 8908–8918, Nov. 2017.

[116] E. Afshari, B. Farhangi, Y. Yang, and S. Farhangi, "A low-voltage ride-through control strategy for three-phase grid-connected PV systems," in *Proc. IEEE Power Energy Conf. Illinois (PECI)*, Champaign, IL, USA, Feb. 2017, pp. 1–6.

[117] E. Afshari, G. R. Moradi, Y. Yang, B. Farhangi, and S. Farhangi, "A review on current reference calculation of three-phase grid-connected PV converters under grid faults," in *Proc. IEEE Power Energy Conf. Illinois (PECI)*, Champaign, IL, USA, Feb. 2017, pp. 1–7.

[118] J. J. Joshi and A. K. V. Swami Jately, "Active power curtailment in PV array under LVRT condition," in *Advances in Intelligent Systems and Computing*. Singapore, Springer, 2021, pp. 65–74.

[119] P. Shah and B. Singh, "Low-voltage ride-through operation of grid interfaced solar PV system enabling harmonic compensation capabilities," *IET Renew. Power Gener.*, vol. 14, no. 12, pp. 2100–2113, Sep. 2020.

[120] M. A. Garnica Lopez, J. L. Garcia de Vicuna, J. Miret, M. Castilla, and R. Guzman, "Control strategy for grid-connected three-phase inverters during voltage sags to meet grid codes and to maximize power delivery capability," *IEEE Trans. Power Electron.*, vol. 33, no. 11, pp. 9360–9374, Nov. 2018.

[121] H. Dehghani Tafti, A. I. Maswood, G. Konstantinou, J. Pou, and P. Acuna, "Active/reactive power control of photovoltaic grid-tied inverters with peak current limitation and zero active power oscillation during unbalanced voltage sags," *IET Power Electron.*, vol. 11, no. 6, pp. 1066–1073, Mar. 2018.

[122] M. G. Taul and X. Wang, "Current reference generation based on next generation grid code requirements of grid-tied converters during asymmetrical faults," *IEEE Trans. Emerg. Sel. Topics Power Electron.*, vol. 8, no. 4, pp. 3784–3797, Jul. 2019.

[123] D. Çelik and M. E. Meral, "A novel control strategy for grid connected distributed generation system to maximize power delivery capability," *Energy*, vol. 186, Nov. 2019, Art. no. 115850.

[124] D. Çelík and M. E. Meral, "A flexible control strategy with overcurrent limitation in distributed generation systems," *Int. J. Electr. Power Energy Syst.*, vol. 104, pp. 456–471, Jan. 2019.

[125] J. L. Sosa, M. Castilla, J. Miret, J. Matas, and Y. A. Al-Turki, "Control strategy to maximize the power capability of PV three-phase inverters during voltage sags," *IEEE Trans. Power Electron.*, vol. 31, no. 4, pp. 3314–3323, Apr. 2016.

[126] M. A. G. Lopez, L. G. de Vicuna, J. Miret, P. Marti, and M. Velasco, "Control strategy to maximize the power capability of PV-based industrial microgrids during voltage sags," in *Proc. 43rd Annu. Conf. Ind. Electron. Soc.*, Beijing, China, Oct. 2017, pp. 1001–1006.

[127] M. Mirhosseini, J. Pou, and V. G. Agelidis, "Single and two-stage inverter-based grid-connected photovoltaic power plants with ride-through capability under grid faults," *IEEE Trans. Sustain. Energy*, vol. 6, no. 3, pp. 1–10, Sep. 2014.

[128] M. Mirhosseini, J. Pou, and V. G. Agelidis, "Single-stage inverter-based grid-connected photovoltaic power plant with ride-through capability over different types of grid faults," in *Proc. 39th Annu. Conf. Ind. Electron. Soc.*, Vienna, Austria, Nov. 2013, pp. 8008–8013.

[129] V. Jately, S. Bhattacharya, B. Azzopardi, A. Montgareuil, J. Joshi, and S. Arora, "Voltage and current reference based MPPT under rapidly changing irradiance and load resistance," *IEEE Trans. Energy Convers.*, vol. 36, no. 3, pp. 2297–2309, Sep. 2021.

[130] M. Davari and Y. A.-R. I. Mohamed, "Dynamics and robust control of a grid-connected VSC in multiterminal DC grids considering the instantaneous power of DC and AC side filters and DC grid uncertainty," *IEEE Trans. Power Electron.*, vol. 31, no. 3, pp. 1942–1958, Mar. 2016.

[131] F. Yang, L. Yang, and X. Ma, "An advanced control strategy of PV system for low-voltage ride-through capability enhancement," *Solar Energy*, vol. 109, pp. 24–35, Nov. 2014.

[132] S. Mohamed, P. Jeyanthy, D. Devaraj, M. Shwehdi, and A. Aldalbahi, "DC-link voltage control of a grid-connected solar photovoltaic system for fault ride-through capability enhancement," *Appl. Sci.*, vol. 9, no. 5, p. 952, Mar. 2019.

[133] Y.-S. Lai, Y.-K. Lin, and C.-W. Chen, "New hybrid pulsewidth modulation technique to reduce current distortion and extend current reconstruction range for a three-phase inverter using only DC-link sensor," *IEEE Trans. Power Electron.*, vol. 28, no. 3, pp. 1331–1337, Mar. 2013.

[134] R. Picas, S. Ceballos, J. Pou, J. Zaragoza, G. Konstantinou, and V. G. Agelidis, "Closed-loop discontinuous modulation technique for capacitor voltage ripples and switching losses reduction in modular multilevel converters," *IEEE Trans. Power Electron.*, vol. 30, no. 9, pp. 4714–4725, Sep. 2015.
[135] J. M. S. Callegari, A. F. Cupertino, V. N. Ferreira, E. M. S. Brito, V. F. Mendes, and H. A. Pereira, "Adaptive DC-link voltage control strategy to increase PV inverter lifetime," *Microelectron. Rel.*, vols. 100–101, Sep. 2019, Art. no. 113439.
[136] A. Merabet, L. Labib, A. M. Ghias, C. Ghenai, and T. Salameh, "Robust feedback linearizing control with sliding mode compensation for a grid-connected photovoltaic inverter system under unbalanced grid voltages," *IEEE J. Photovolt.*, vol. 7, no. 3, pp. 828–838, Mar. 2017.
[137] F. Zheng, Y. Chen, T. Ye, Y. Zhang, F. Guo, and Y. Zhang, "Design of hybrid control algorithm for fault ride-through of photovoltaic system," *IEEE Access*, vol. 7, pp. 124196–124206, 2019.
[138] Y. He, Z. Xu, and Y. Li, "A novel control scheme for enhancing low voltage ride through capability of solar generation," in *Proc. China Int. Electr. Energy Conf. (CIEEC)*, Beijing, China, Oct. 2017, pp. 129–134.
[139] G. B. Huka, W. Li, P. Chao, and S. Peng, "A comprehensive LVRT strategy of two-stage photovoltaic systems under balanced and unbalanced faults," *Int. J. Electr. Power Energy Syst.*, vol. 103, pp. 288–301, Dec. 2018.
[140] L. Wang, T. Qiao, B. Zhao, X. Zeng, and Q. Yuan, "Modeling and parameter optimization of grid-connected photovoltaic systems considering the low voltage ride-through control," *Energies*, vol. 13, no. 15, p. 3972, Aug. 2020.
[141] A. Merabet, L. Labib, and A. M. Y. M. Ghias, "Robust model predictive control for photovoltaic inverter system with grid fault ride-through capability," *IEEE Trans. Smart Grid*, vol. 9, no. 6, pp. 5699–5709, Nov. 2018.
[142] Y. Gui, F. Blaabjerg, X. Wang, J. D. Bendtsen, D. Yang, and J. Stoustrup, "Improved DC-link voltage regulation strategy for grid-connected converters," *IEEE Trans. Ind. Electron.*, vol. 68, no. 6, pp. 4977–4987, Jun. 2021.
[143] S. Fahad, A. J. Mahdi, W. H. Tang, K. Huang, and Y. Liu, "Particle swarm optimization based DC-link voltage control for two stage grid connected PV inverter," in *Proc. Int. Conf. Power Syst. Technol. (POWERCON)*, Guangzhou, China, Nov. 2018, pp. 2233–2241.
[144] N. Aouchiche, "Meta-heuristic optimization algorithms based direct current and DC link voltage controllers for three-phase grid connected photovoltaic inverter," *Sol. Energy*, vol. 207, pp. 683–692, Sep. 2020.
[145] G. Ding, F. Gao, J. China, H. Tian, C. Ma, M. Chen, G. He, and Y. Liu, "Adaptive DC-link voltage control of two-stage photovoltaic inverter during low voltage ride-through operation," *IEEE Trans. Power Electron.*, vol. 31, no. 6, pp. 4182–4194, Jun. 2016.
[146] C. Jain and B. Singh, "An adjustable DC link voltage-based control of multifunctional grid interfaced solar PV system," *IEEE Trans. Emerg. Sel. Topics Power Electron.*, vol. 5, no. 2, pp. 651–660, Nov. 2016.
[147] C. Jain and B. Singh, "A three-phase grid tied SPV system with adaptive DC link voltage for CPI voltage variations," *IEEE Trans. Sust. Energy*, vol. 7, no. 1, pp. 337–344, Nov. 2015.
[148] M. Merai, M. W. Naouar, and I. Slama-Belkhodja, "An improved DC-link voltage control strategy for grid connected converters," *IEEE Trans. Power Electron.*, vol. 33, no. 4, pp. 3575–3582, Apr. 2018.
[149] H. Wen and M. Fazeli, "A new control strategy for low-voltage ride-through of three-phase grid-connected PV systems," *J. Eng.*, vol. 2019, no. 18, pp. 4900–4905, Jul. 2019.
[150] M. A. Shuvra and B. Chowdhury, "Distributed dynamic grid support using smart PV inverters during unbalanced grid faults," *IET Renew. Power Gener.*, vol. 13, no. 4, pp. 598–608, Mar. 2019.
[151] Y. He, M. Wang, Y. Jia, J. Zhao, and Z. Xu, "Low-voltage ride-through control for photovoltaic generation in the low-voltage distribution network," *IET Renew. Power Gener.*, vol. 14, no. 14, pp. 2727–2737, Oct. 2020.
[152] H. Khan, S. J. Chacko, B. G. Fernandes, and A. Kulkarni, "Reliable and effective ride-through controller operation for smart PV systems connected to LV distribution grid under abnormal voltages," *IEEE J. Emerg. Sel. Topics Power Electron.*, vol. 8, no. 3, pp. 2371–2384, Sep. 2020.
[153] T. Zhao and D. Chen, "Active power backflow control strategy for cascaded photovoltaic solid state transformer during low voltage ride through," *IEEE Trans. Ind. Electron.*, early access, Jan. 20, 2021, doi: 10.1109/TIE.2021.3051592.
[154] F.-J. Lin, K.-H. Tan, W.-C. Luo, and G.-D. Xiao, "Improved LVRT performance of PV power plant using recurrent wavelet fuzzy neural network control for weak grid conditions," *IEEE Access*, vol. 8, pp. 69346–69358, 2020.
[155] S. Bagchi, D. Chatterjee, R. Bhaduri, and P. K. Biswas, "An improved low-voltage ride-through (LVRT) strategy for PV-based grid connected inverter using instantaneous power theory," *IET Gener., Transmiss. Distrib.*, vol. 15, no. 5, pp. 883–893, Mar. 2021.
[156] Z. Shao, X. Zhang, F. Wang, R. Cao, and H. Ni, "Analysis and control of neutral-point voltage for transformerless three-level PV inverter in LVRT operation," *IEEE Trans. Power Electron.*, vol. 32, no. 3, pp. 2347–2359, Mar. 2017.
[157] A. V. Jouanne, S. Dai, and H. Zhang, "A multilevel inverter approach providing DC-link balancing, ride-through enhancement, and common-mode voltage elimination," *IEEE Trans. Ind. Electron.*, vol. 49, no. 4, pp. 739–745, Aug. 2002.
[158] R. Maheshwari, S. Munk-Nielsen, and S. Busquets-Monge, "Design of neutral-point voltage controller of a three-level NPC inverter with small DC-link capacitors," *IEEE Trans. Ind. Electron.*, vol. 60, no. 5, pp. 1861–1871, May 2013.

JYOTI JOSHI received the B.Tech. degree in electrical and electronics engineering from Uttarakhand Technical University (UTU), India, in 2011, and the M.Tech. degree from IFTM University, India, in 2015. She is currently pursuing the Ph.D. degree in electrical engineering with G. B. Pant University of Agriculture and Technology, Pantnagar. She has over seven years of teaching experience during which she also served as a Lecturer under United Nations Development Programme in Ethiopia. Her research interests include current controllers in grid-connected photovoltaic systems, fault ride through in grid-connected photovoltaic systems, and flexible power point tracking in photovoltaic systems.

ANURAG KUMAR SWAMI received the B.Tech. degree in electrical engineering and the M.Tech. degree (control system) from the NIT Kurukshetra, India, in 1981 and 1986, respectively, and the Ph.D. degree in electrical engineering from the College of Technology, G. B. Pant University, Pantnagar, India, in 2004. He has over 30 years of teaching experience and five years of industrial experience. His research interest includes control and instrumentation.

VIBHU JATELY (Member, IEEE) received the Ph.D. degree in electrical engineering from the College of Technology, G. B. Pant University, Pantnagar, India, in 2017. He has over six years of research and teaching experience during which he has also worked under United Nations Development Programme in Ethiopia. Since July 2019, he has been working as a Postdoctoral Research Fellow with MCAST Energy Research Group, MCAST, Malta. His research interests include control in photovoltaic systems, control in power electronics, and grid-connected photovoltaic systems.

BRIAN AZZOPARDI (Senior Member, IEEE) received the B.Eng. degree from the University of Malta, in 2002, and the Ph.D. degree from The University of Manchester, U.K., in 2011. He currently holds a senior academic position with Malta College of Arts, Science and Technology (MCAST) and leads the Energy Research Group, and a Visiting Senior Lecturer with the University of Malta. His research interests include photovoltaics and electric mobility network integration, and future urban low-carbon society.